Department of Applied Physics

Bloch line dynamics within magnetic domain walls

Touko Herranen

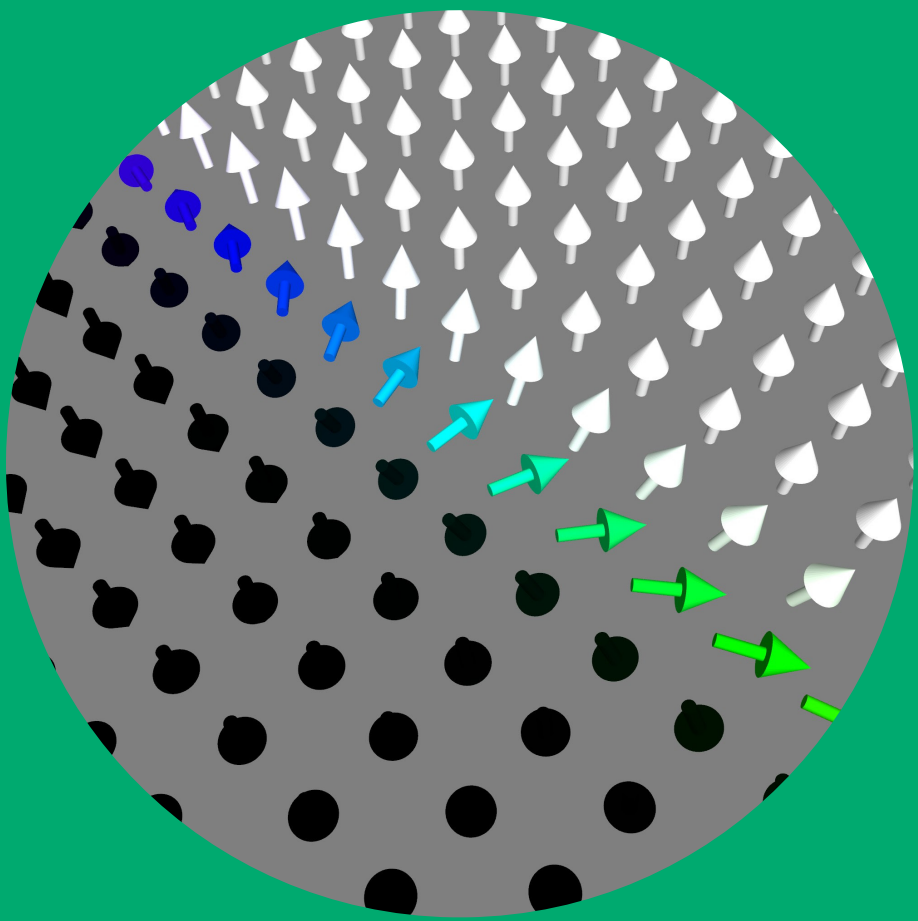

Aalto University

DOCTORAL DISSERTATIONS

Aalto University publication series
DOCTORAL DISSERTATIONS 153/2018

Bloch line dynamics within magnetic domain walls

Touko Herranen

A doctoral dissertation completed for the degree of Doctor of Science (Technology) to be defended, with the permission of the Aalto University School of Science, at a public examination held at the lecture hall M1 of the school on 7th September 2018 at 13.

Aalto University
School of Science
Department of Applied Physics
Complex Systems and Materials

Supervising professor
Professor Mikko Alava, Aalto University, Finland

Thesis advisor
Dr. Lasse Laurson, Aalto University, Finland

Preliminary examiners
Professor Luis López Díaz, University of Salamanca, Spain
PhD Jan Vogel, Institut Néel, France

Opponent
Dr. Gianfranco Durin, Istituto Nazionale di Ricerca Metrologica, Italy

Aalto University publication series
DOCTORAL DISSERTATIONS 153/2018

ISBN 978-952-60-8133-5 (printed)
ISBN 978-952-60-8134-2 (pdf)
ISSN 1799-4934 (printed)
ISSN 1799-4942 (pdf)
http://urn.fi/URN:ISBN:978-952-60-8134-2

Unigrafia Oy
Helsinki 2018

Finland

441 697
Printed matter

Aalto University

Abstract

Aalto University, P.O. Box 11000, FI-00076 Aalto www.aalto.fi

Author
Touko Herranen

Name of the doctoral dissertation
Bloch line dynamics within magnetic domain walls

Publisher School of Science

Unit Department of Applied Physics

Series Aalto University publication series DOCTORAL DISSERTATIONS 153/2018

Field of research Theoretical and Computation Physics

Manuscript submitted 15 August 2018 **Date of the defence** 7 September 2018

Permission to publish granted (date) 15 August 2018 **Language** English

☐ **Monograph** ☒ **Article dissertation** ☐ **Essay dissertation**

Abstract

Magnetic domains are uniformly magnetized regions within a ferromagnet separated by magnetic domain walls. The internal degrees of freedom of a domain wall can be excited by applying a magnetic field greater than so called Walker field. As a result the domain wall velocity experiences the Walker breakdown, an abrupt drop of the average velocity, and the magnetization of the domain wall starts a cyclic rotation. If this mechanism is triggered in a domain wall with a dimension greater than a material characteristic Bloch line width, the excitations become non-uniform, which results in nucleation of domain walls within the domain wall called Bloch lines. The dynamics of domain walls in disordered media have been studied extensively using various computational methods as well as experimentally. In this doctoral dissertation we use a micromagnetics software to simulate the Bloch line dynamics and the effects of Bloch lines on domain wall dynamics in samples with perpendicular magnetic anisotropy.

In Publication I we study the domain wall dynamics in CoPtCr thin films with different widths. We observe nucleation of Bloch lines within domain walls in disordered and perfect samples when driven with a magnetic field higher than the Walker field. We construct a geometry to confine the domain wall between two notches, and use it to study Bloch line dynamics under an in-plane field. Finally we demonstrate the performance potential of an electrical current operated Bloch line memory.

In Publication II we study the effects of boundary conditions and thickness effects on the domain wall dynamics in a magnetic garnet, and we find they determine the internal dynamics allowed for the magnetization of the domain wall. The sample thickness limits the maximum achievable stable velocity before the breakdown. The velocity limit is also found to be related to the spatial width of Bloch lines.

In Publication III we use a micromagnetics approach to study the Barkhausen effect and avalanche statistics in a thin Pt/Co/Pt multilayer. The domain wall is driven using a quasistatic constant velocity. The novel approach enables us to determine magnetization of the domain wall segment where avalanches are triggered. Internal magnetization dynamics show that during avalanches the activity of in-plane magnetization, i.e. the Bloch line motion, is higher than the activity related to the domain wall motion. Avalanche size and duration distributions obtained from the activity signals follow power law scaling, and the corresponding features extracted from the domain wall velocity show no significant difference. The analysis also shows that the results obtained using micromagnetic simulations are close to the values expected from a simpler model describing a short-range elastic string in a random medium.

Keywords micromagnetics, domain wall dynamics, Bloch lines, Barkhausen noise

ISBN (printed) 978-952-60-8133-5 **ISBN (pdf)** 978-952-60-8134-2

ISSN (printed) 1799-4934 **ISSN (pdf)** 1799-4942

Location of publisher Helsinki **Location of printing** Helsinki **Year** 2018

Pages 85 **urn** http://urn.fi/URN:ISBN:978-952-60-8134-2

Aalto-yliopisto

Tiivistelmä

Aalto-yliopisto, PL 11000, 00076 Aalto www.aalto.fi

Tekijä
Touko Herranen

Väitöskirjan nimi
Magneettisen seinämän Bloch-viivojen dynamiikka

Julkaisija Perustieteiden korkeakoulu

Yksikkö Teknillisen fysiikan laitos

Sarja Aalto University publication series DOCTORAL DISSERTATIONS 153/2018

Tutkimusala Teoreettinen ja laskennallinen fysiikka

Käsikirjoituksen pvm 15.08.2018 **Väitöspäivä** 07.09.2018

Julkaisuluvan myöntämispäivä 15.08.2018 **Kieli** Englanti

☐ **Monografia** ☒ **Artikkeliväitöskirja** ☐ **Esseeväitöskirja**

Tiivistelmä

Ferromagneetissa on magneettisia alueita, joissa atomien magneettiset momentit ovat samansuuntaiset ja joita erottaa magneettinen seinämä. Seinämän sisäiset vapausasteet voidaan virittää asettamalla se ulkoiseen magneettikenttään, jonka voimakkuus on suurempi kuin niin kutsutun Walkerin kentän. Tämän seurauksena seinämä kokee Walkerin romahduksen, mikä ilmenee keskimääräisen nopeuden romahduksena ja seinämän magnetisaatio alkaa kiertyä syklisesti. Jos mekanismi käynnistetään magneettisessa seinämässä, jonka jokin ulottuvuus on suurempi kuin materiaalille tyypillinen Bloch-viivan pituus, magneettisen seinämän sisään muodostuu seinämiä joita kutsutaan Bloch-viivoiksi. Magneettisten seinämien dynamiikkaa on tutkittu laajasti sekä käyttäen erinäisiä laskennallisia menetelmiä että kokeellisesti. Tässä väitöskirjassa käytämme mikromagneettista ohjelmistoa tutkiaksemme Bloch-viivojen dynamiikka sekä niiden vaikutusta seinämien dynamiikkaan kohtisuoran magneettisen anisotropian näytteissä.

Ensimmäisessä julkaisussa tutkimme eri levyisten CoPtCr-ohutkalvojen seinämän dynamiikkaa. Havaitsemme Bloch-viivojen nukleaatiota seinämissä sekä epäjärjestyneissä että puhtaissa näytteissä, kun ulkoinen kenttä on asetettu Walkerin kenttää voimakkaammaksi. Luomme järjestelyn, joka rajoittaa seinämän kahden loven väliin, ja käytämme sitä tutkiaksemme Bloch-viivojen dynamiikkaa pinnan suuntaisen kentän vaikutuksen alaisena. Lopuksi demonstroimme sähkövirralla ajetun Bloch-viivamuistin potentiaalista suorituskykyä.

Toisessa julkaisussa tutkimme reunaehtojen ja näytteen paksuuden vaikutusta seinämän dynamiikkaan magneettisessa granaatissa, ja huomaamme että nämä ominaisuudet määrittävät seinämän sisäistä dynamiikkaa. Näytteen paksuus rajoittaa seinämän suurinta vakaan dynamiikan nopeutta ennen romahdusta. Huomaamme myös maksiminopeuden kytkeytyvän Bloch-viivojen leveyteen.

Kolmannessa julkaisussa lähestymme Barkhausenin kohinaa ja vyörystatistiikkaa ohuissa Pt/Co/Pt kerrosrakenteissa mikromagnetismin keinoin. Seinämää kuljetetaan käyttäen kvasistaattista vakionopeutta. Uudenlainen lähestymistapa mahdollistaa ensimmäistä kertaa magnetisaation havaitsemisen seinämän osasta, josta vyöry on saanut alkunsa. Seinämän magnetisaation sisäinen dynamiikka osoittaa, että Bloch-viivojen aktiivisuus on voimakkaampaa vyöryjen aikana kuin itse seinämän etenemiseen liittyvä aktiivisuus. Aktiivisuussignaaleista määritetyt vyöryjen koko- ja kestojakaumat noudattavat potenssilakia, ja vastaavat piirteet ovat havaittavissa myös seinämän nopeudesta määritetyissä jakaumissa. Analyysi osoittaa myös että mikromagneettisista simulaatioista saadut tulokset ovat lähellä pelkistetymmällä mallilla saatuja tuloksia. Pelkistetty malli kuvaa lyhyen kantaman vuorovaikutuksia elastisessa langassa epäpuhtaassa väliaineessa.

Avainsanat mikromagnetismi, magneettiset seinämät, Bloch-viivat, Barkhausenin kohina

ISBN (painettu) 978-952-60-8133-5 **ISBN (pdf)** 978-952-60-8134-2

ISSN (painettu) 1799-4934 **ISSN (pdf)** 1799-4942

Julkaisupaikka Helsinki **Painopaikka** Helsinki **Vuosi** 2018

Sivumäärä 85 **urn** http://urn.fi/URN:ISBN:978-952-60-8134-2

Preface

The doctoral research process has been a journey into myself and into the fascinating world of science, which I started dreaming about during the high school when I was reading popular science magazines. My academic studies, which started in 2007, have now come to an end and this doctoral dissertation is both my reward and my accomplishment. I have been a part of the scientific community and have met a lot of wonderful people along the way. Very few of us can achieve great things alone and I am not an exception here, but I have received guidance, support and help from excellent people.

When I started working in Complex Systems and Materials group (CSM), led by professor Mikko Alava, approximately 5 years ago I was a bachelor of science and made a comeback to the academy after spending a year in the industry. Culture shock was extreme because a mere visualization of the data was not enough, but the ideas were expected to be presented in an exact manner and all matters affecting phenomena considered. The atmosphere in CSM group has been great and humor has been part of the everyday life – even the best kind of humor which is the black humor. Thank you, Mikko, for standing up for your employees and for making the atmosphere pleasant for us all.

I started my dive into research by doing simulations with a model based on the Ising model. My master's thesis concerning magnetic domain walls was conducted under a firm instruction of Dr. Lasse Laurson. It was time to start the doctoral research after the graduation as a master of science. At first the amount of work felt vague and enormous. Me and Lasse were looking at the animations of my first micromagnetic simulations and we found a substructure within a magnetic domain wall, which was unfamiliar to both of us. Later we found out that the object was a well-known topological defect – Bloch-line, which had been thoroughly studied theoretically in the 1970s and 80s. Eventually, I ended up studying the dynamics of Bloch-lines in different geometries and samples, the effect of Bloch-lines on magnetic domain wall dynamics and writing my doctoral dissertation about them. Thank you, Lasse, for collaboration, your work as an instructor, lunch company and arrangement of funding. This dissertation would not exist without you.

I want to thank all the former and present colleagues in CSM-group, whom

I have travelled with and celebrated BBQs and pre-Christmas parties. The discussions have been diverse and fruitful, and there has been a lot of laughter involved in these events as well. I also learned a card game from our group, which is the first card game I don't actually like but nevertheless it is played at all events of our group. Especially I would like to thank my former colleague, Dr. Arttu Lehtinen, for the coffee break and lunch discussions. These moments away from the computer were the highpoints of my workdays. Partly thanks to Arttu I also got my job to do research under Lasse.

The life outside of academy is also indirectly connected with the thesis work. I have spent my free time together with wonderful people it has brought a lot of pleasure to my life. We have had a lot of different celebrations, events, trips and game nights. I would like to thank my fellow students as well as my childhood friends, the Truckers, for the awesome adventures.

I would like to thank my mother, Paula, for warm and safe childhood. My father, Kyösti, I thank for unquestionable support for the choices I have made, bike trips together, computers you have bought, and for everything else you have done for me. Thanks to my sister, Sonja, and my brother, Kosti, for the trips to summer cottages and other celebrations, which have brought a nice counterbalance to the research work. I also want to thank you two for the IT-support that you provided when I was a very young boy. I want to thank the spouses and offspring of my family members for all the good times together. I would like to show my gratitude to my wife's family Riitta, Jukka and Katri, as well as to their spouses for the help taking care of the kids and all the time we have spent together. You have literally kept our house standing.

I haven't needed an alarm clock for the last three years, but instead I have been woken up by our beloved children Tauno and Liina. Just seeing your smile and happiness made waking up easy in the morning and you made coming back home in the evening feel like a celebration. And finally, I would like to express my greatest gratitude to my muse and my wife, Noora. Thank you for your support, taking care of the children when I was under a tight schedule, steaming food waiting for me when I have arrived home from work, coping during the roughest times and for all the motivation you have given me. I can at each moment trust thou.

And same in Finnish.

Väitöskirjaprosessi on ollut matka omaan itseeni ja samalla sukellus kiehtovaan tieteelliseen maailmaan, josta aloin haaveilla yläasteella tiedelehtiä lukiessani. Vuonna 2007 alkaneet yliopisto-opintoni ovat nyt tulleet päätökseensä ja tämä väitöskirja on sekä palkintoni että työni tulos. Olen päässyt osaksi hienoa tieteellistä yhteisöä ja tavannut upeita ihmisiä matkan varrella. Harva ihminen pystyy saavuttamaan suuria asioita yksinään enkä minäkään ole poikkeus vaan olen saanut ohjausta, tukea ja apua näiltä upeilta ihmisiltä.

Aloittaessani työskentelyn professori Mikko Alavan johtamassa Complex sys-

tems and materials -ryhmässä (CSM) n. 5 vuotta sitten olin luonnontieteiden kandidaatti ja saavuin takaisin tieteen pariin yritysmaailmassa vietetyn vuoden jälkeen. Kulttuurishokki oli melkoinen, sillä enää ei riittänyt pelkkä tulosten visualisointi, vaan asiat tuli esittää eksaktisti perustellen ja kaikki havaittuihin ilmiöihin vaikuttavat tekijät huomioon ottaen. CSM-ryhmässä on ollut hyvä ryhmähenki ja huumoria on viljelty kosolti – myös sitä parasta huumoria eli mustaa. Kiitos Mikko, että olet pitänyt omiesi puolta ja tehnyt työympäristöstämme miellyttävän meille kaikille.

Aloitin tutkimukseen perehtymisen tekemällä Ising-malliin pohjautuvia simulaatioita. Magneettista rajapintaa käsittelevän pro gradu -tutkielmani tein tohtori Lasse Laursonin jämäkässä ohjauksessa. Maisteriksi valmistumisen jälkeen oli aika aloittaa väitöskirjatutkimus, mikä tuntui aluksi epämääräiseltä ja valtavalta työmäärältä. Katsellessamme Lassen kanssa ensimmäisiä mikromagnetismisimulaatioitteni tuloksia havaitsimme meille molemmille tuntemattoman alirakenteen magneettisessa seinämässä. Myöhemmin meille selvisi, että kyseessä on hyvinkin tunnettu topologinen defekti – Bloch-viiva, josta oli kirjoitettu paljon teoreettisia tuloksia 70- ja 80-luvuilla. Lopulta päädyin tutkimaan juuri kyseisten objektien dynamiikkaa erilaisissa geometrioissa ja näytteissä, Bloch-viivojen vaikutusta magneettisen rajapinnan dynamiikkaan sekä kirjoittamaan väitöskirjani niistä. Kiitokset Lasse ohjauksestasi, yhteistyöstä, lounasseurasta ja rahoituksen järjestämisestä. Ilman sinua tätä väitöskirjaa ei olisi olemassakaan.

Haluan myös kiittää myös koko CSM-ryhmän entisiä ja nykyisiä kollegoja, joiden kanssa olemme matkustaneet sekä viettäneet grillijuhlia ja pikkujouluja. Keskustelut ovat olleet monipuolisia ja hedelmällisiä eikä näistäkään tilaisuuksista ole nauru jäänyt puuttumaan. Opin ryhmältämme myös ensimmäisen korttipelin, josta en pidä mutta sitä määrätietoisesti pelataan jokaisessa ryhmän tapahtumassa. Erityisesti haluan kiittää entistä kollegaani tohtori Arttu Lehtistä yhteisistä kahvi- ja lounaskeskusteluista. Nämä ajoittaiset irrottautumiset tietokoneen ääreltä olivat ehdottomasti työpäivien kohokohtia. Osittain Artun ansiosta sain myös työpaikan Lassen alaisuudessa.

Epäsuorasti väitöskirjatyöhön liittyy myös tieteellisen maailman ulkopuolella tapahtuva elämä. Vapaa-aikaani olen viettänyt hienojen ihmisten kanssa ja tämä yhteinen aika on myös tuonut merkittävästi lisää sisältöä elämään erilaisten juhlien, tapahtumien, matkojen ja peli-iltojen muodossa. Haluaisin kiittää opiskelukavereitani sekä lapsuudenystäviäni, Rekkamiehiä, kaikista mahtavista seikkailuista.

Haluan kiittää äitiäni, Paulaa, pullantuoksuisesta ja turvallisesta lapsuudesta. Isääni, Kyöstiä, kiitän järkkymättömästä tuesta valintojani kohtaan, yhteisistä pyörämatkoista, tietokoneista, sekä kaikesta muusta mitä olet eteeni tehnyt. Kiitokset siskolleni Sonjalle ja veljelleni Kostille mökkireissuista ja juhlista, jotka ovat tuoneet mukavaa vastapainoa työlle. Haluan myös kiittää teitä IT-tuesta, jota annoitte minulle jo hyvin varhaisella iällä. Kiitokset myös perheenjäsenteni puolisoille ja jälkeläisille mukavista viikonlopuista yhdessäolon

merkeissä. Suuret kiitokset osoitan myös puolisoni perheelle Riitalle, Jukalle ja Katrille sekä heidän kumppaneilleen avusta lastenhoidossa ja kaikista yhteisistä hetkistä. Olette pitäneet kotimme pystyssä sanan kaikissa merkityksissä.

Viimeisen kolmen vuoden aikana en ole juurikaan tarvinnut herätyskelloa, vaan minut ovat herättäneet rakkaat lapsemme Tauno ja Liina. Hymynne ja iloisuutenne ovat auttaneet aamuisin heräämään ja iltaisin saaneet kotiintulon tuntumaan juhlalta. Lopuksi haluaisin osoittaa suurimmat kiitokset muusalleni ja rakkaalle vaimolleni, Nooralle. Kiitos tuesta, motivoinnista, lasten hoitamisesta tiukkojen aikataulujen painaessa päälle, lämpimästä ruoasta iltaisin kotiin tullessa sekä jaksamisesta rankkoinakin aikoina. Sinuun voin aina luottaa.

Espoo, August 16, 2018,

Touko Herranen

Contents

List of Publications

This thesis consists of an overview and of the following publications which are referred to in the text by their Roman numerals.

I Touko Herranen and Lasse Laurson. Domain walls within domain walls in wide ferromagnetic strips. *Physical Review B*, 92, 100405(R), September 2015.

II Touko Herranen and Lasse Laurson. Bloch-line dynamics within moving domain walls in 3D ferromagnets. *Physical Review B*, 96, 144422, October 2017.

III Touko Herranen and Lasse Laurson. Barkhausen noise from precessional domain wall motion. Submitted to *Physical Review Letters*, June 8th 2018.

Author's Contribution

Publication I: "Domain walls within domain walls in wide ferromagnetic strips"

The author did the simulations, analysis, figures and wrote the first draft of the manuscript.

Publication II: "Bloch-line dynamics within moving domain walls in 3D ferromagnets"

The author did the simulations, analysis, figures and wrote the first draft of the manuscript.

Publication III: "Barkhausen noise from precessional domain wall motion"

The author did the simulations, analysis, figures and wrote the first draft of the manuscript.

List of Abbreviations

BL	Bloch line
DW	Domain wall
HBL	Horizontal Bloch line
H2H	Head-to-head
PBC	Periodic boundary conditions
PMA	Perpendicular magnetic anisotropy
OBC	Open boundary conditions
T2T	Tail-to-Tail
VBL	Vertical Bloch line

List of Symbols

A_{ex}	Exchange stiffness, [J/m]
α	Gilbert damping parameter, [1]
B_{dep}	Depinning field, [T]
B_{ext}	External magnetic field, [T]
B_{W}	Walker field, [T]
C	Chirality, [1]
Δ_{DW}	Bloch wall width parameter, [m]
j_{W}	Walker current density, [A/m^2]
K_{u}	Uniaxial anisotropy, [J/m^3]
Λ	Bloch line width parameter, [m]
$\mathbf{m}$	Magnetization vector, [1]
M_{S}	Saturation magnetization, [A/m]
μ	Mobility, [(m/s)/T]
μ_0	Vacuum permeability, [Tm/A]
Q	Topological charge, [1]
S	Avalanche size, [a.u.]
T	Avalanche duration, [s]
v, v_{DW}	Domain wall velocity, [m/s]
ξ	Nonadiabatic parameter, [1]

1. Introduction

Ferromagnets are materials that have a spontaneous magnetization when temperature is below a material characteristic Curie temperature. They can be permanently magnetized by applying an external magnetic field and at the point where all magnetic moments or "spins" are aligned with the applied field the material has reached its saturation magnetization M_S. If the applied field is removed the fraction of the retained magnetization is called remanence of the material. Ferromagnetic behavior can be removed by heating a sample over its Curie temperature [1].

Other kinds of magnetism that materials can exhibit are diamagnetic, paramagnetic, antiferromagnetic and ferrimagnetic. All substances are magnetic to some extent but diamagnetic, paramagnetic and antiferromagnetic materials are usually called non-magnetic for the reason that they cannot be turned into permanent magnets. Visualization of the magnetic order in these material types is presented in Fig. 1.1. Furthermore, the magnetic materials can be divided into two groups: the magnetically soft and hard materials. Magnetically soft materials are easy to magnetize and demagnetize and hard magnetic materials are hard to magnetize and demagnetize. Soft magnetic materials have high permeability and mainly for that reason are used as flux multipliers in industry applications. Hard magnetic materials have high coercivity, which is the field needed to demagnetize the material and high coercivity is a primary prerequisite for a permanent magnet. Hard magnets resist well the demagnetizing effect of stray fields, including their own [1].

Ferromagnetic materials exhibit a long-range ordering phenomenon, which causes the unpaired electron spins to align with each other. Magnetic domains are regions within ferromagnets that are uniformly magnetized. Magnetic domains with different magnetization direction are separated by a region called magnetic domain wall (DW) [2]. The process where domain magnetization is reoriented can either be based on the displacement of DWs or rotation of magnetization of the entire domain magnetization [2]. Spin magnetizations within a domain might be parallel, but on the other hand the net magnetization of the ferromagnet may be negligible, because the domains can have random magnetization across the whole sample. An example of a domain structure with

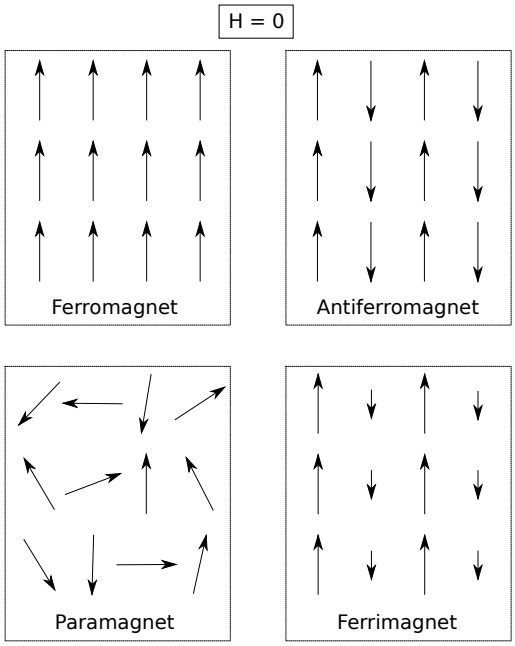

Figure 1.1. Schematics of the magnetization within magnetic materials in zero field.

the total z component of magnetization $m_z \approx 0$ is presented in Fig. 1.2. Tendency of the spins to organize into domains and align with the so-called easy crystal axis is caused by the crystal anisotropy of the material. Due to the exchange effect of quantum-mechanical origin, the magnetization **m** cannot just rotate e.g. 180° from domain to another but it rotates in finite steps, spin by spin, resulting in a DW of finite width [2].

Depending on the anisotropy the magnetization of the domains can be either in-plane or out of the material plane. In this dissertation I focus on materials with out-of-plane magnetization, which can also be referred as perpendicular magnetic anisotropy (PMA) materials [2].

Magnetization of materials can be manipulated by e.g. applying a magnetic field or an electric current. If magnetic switching is carried out by generating magnetic field according to Ampère's law, the needed current density increases as the sample size is downscaled. The current-induced magnetization reversal, on the other hand, will operate with a constant current density independent of the system size making it more efficient for small scale applications [3]. Current-induced magnetization reversal is more relevant to memory and logic applications due to this scaling behavior. Current-induced DW motion is caused by spin angular momentum carried by the conduction electrons, which is transferred to the local magnetic moments through the exchange interaction. The conduction electron magnetic moment aligns with the local magnetic moment when the electrons travel through the magnetic domain. As the electrons encounter a domain boundary i.e. DW, they transfer their spin angular momentum

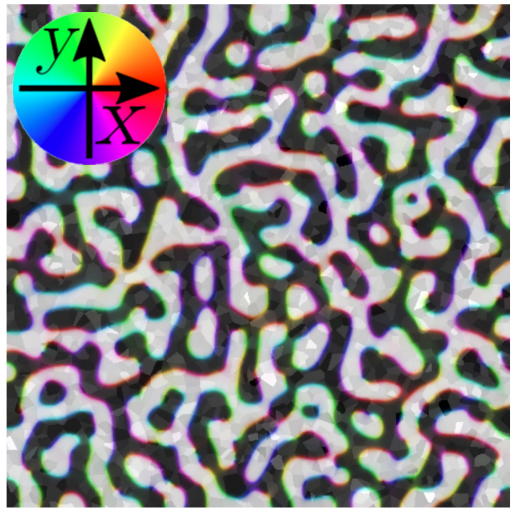

Figure 1.2. Magnetic domains in a PMA strip under a zero field. Thickness of the sample is 40 nm, width and length are 2048 nm. Micromagnetic parameters: saturation magnetization $M_S = 600$ kA/m, uniaxial anisotropy $K_u = 2 \times 10^5\,\mathrm{J/m^3}$, and damping parameter $\alpha = 1.0$. The disorder is implemented by dividing the sample into "grains" using Voronoi tessellation and reducing intergranular exchange interaction by 10 %, randomizing the cubic anisotropy easy axis directions in each grain, and randomizing the first order cubic anisotropy $\langle K_{c1} \rangle = 1 \times 10^5\,\mathrm{J/m^3}$ with standard deviation $\sigma_{K_{c1}} = 1 \times 10^4\,\mathrm{J/m^3}$. The sample parameters are chosen just for demonstration purposes, but the resulting magnetic maze pattern is known to be found in ferromagnets [2]. The domains are separated by domain walls, which are shown in colors. The z component of the magnetization of this structure $m_z \approx 0$ meaning that the area of black and white domains are almost equal. The underlying granular structure is shown in gray scale with a transparent presentation. The color wheel shows the mapping between the in-plane components of the magnetization and the colors. White and black colors correspond to $\pm z$ directions, respectively.

to the local magnetic moments causing spin torque. Continuous flow of the current thus winds the DW in the direction of the electron flow [4].

Now I will briefly introduce the concept of racetrack memory, which is a commercially promising application based on DWs. The racetrack memory was made viable by the discovery made by Stuart Parkin and his co-workers in 2008 [5]. They experimentally proved that magnetic domains can store digital data in their magnetization in nanowires, and DWs could be moved by applying a spin polarized current. They showed that domains move synchronously along the magnetic wire. They suggested, that writing data into racetrack memory could be done by applying a local magnetic field, which would switch the magnetic state of a bit.

Racetrack memories have several advantages compared to traditional ways of storing data in conventional hard drive disks, which can only store one layer of data due to the technique of rotating a disk read by a reading head in the end of a mechanical arm. Racetrack memories could be stacked vertically and form an array of racetrack units. This would bring the data storage into 3D form [6]. It would not have any moving mechanical parts which would extend the memory's lifetime. Racetrack memory could read and write a bit of data into it in 1 to 10 ns depending on the length of the wire, whereas hard drive disks write it typically in 3 ms. A flash drive could store one bit per transistor but racetrack memory could do 100 bits per transistor or more [7].

In the first phase the magnetic racetrack memories were in-plane systems [6]. In soft materials the DW width is mostly determined by the shape anisotropy and thus varies with the wire width. These DWs can be rather wide and to pack data more densely, the magnetization must be out-of-plane. Recently Parkin himself has focused on the layered synthetic antiferromagnetic structures where they have achieved DW velocities as high as 750 m/s [8, 9].

DWs have internal degrees of freedom, which can be excited by exposing the magnetic system to a relatively strong magnetic field or a spin-polarized electric current [10, 11]. Depending on the length of the DW, the excitations are either spatially uniform or non-uniform. In a long DW the excitation of internal degrees of freedom are non-uniform and nucleate "knots" within the magnetization of the DW. These knots are called Bloch lines (BLs). The magnetization of the DW rotates by π radians across a BL dividing the DW into two oppositely magnetized regions. BLs and their effect on DW dynamics were studied in all of my publications discussed in this dissertation.

2. Magnetic structures and dynamics

2.1 Magnetic domains

Magnetic domains are regions where all the magnetic spins point to a uniform direction in ferromagnets [2]. This property is characteristic for ferromagnets when they are cooled below Curie temperature. Domains can also be found in antiferromagnets [12] and ferrimagnets [13]. Exchange interaction is the force that tries to align the neighboring spins and thus is the fundamental force driving the ferromagnets to form magnetic domains. Domains can grow and diminish at the cost of neighboring domains with different orientation. Domains can be grown by applying magnetic field pointing to the same direction as the magnetization of the domain. In this dissertation I will be discussing only materials with domains with out-of-plane magnetization.

2.2 Magnetic domain walls

Magnetic domains are separated by regions called magnetic domain walls (DWs). DWs can be moved by applying an external field B_{ext} or spin polarized current

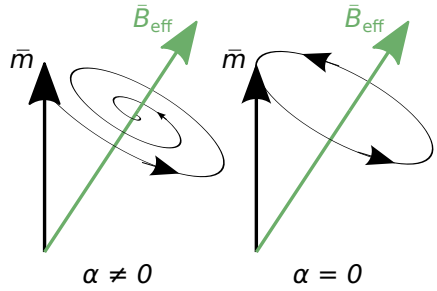

Figure 2.1. Schematic representation of the effect of the Gilbert damping parameter α. Magnetization aligns eventually with the effective field B_{eff} in circular motion, when $\alpha \neq 0$. The magnetic spin rotates around the effective field B_{eff} when $\alpha = 0$.

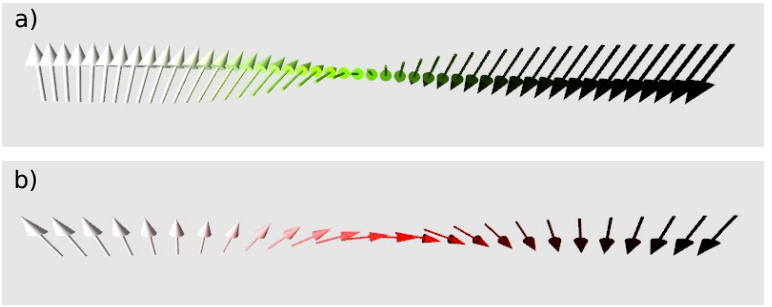

Figure 2.2. One dimensional schematic presentations of magnetization rotations in a Bloch wall in a) and in a Néel wall in b). The rotation of the magnetization changes in small steps, spin-by-spin, and not abruptly from $+z$ (white arrows) to $-z$ (black arrows).

j to the sample. In a single DW system the displacement of the domain wall grows the other magnetic domain while reducing the size of the other. In the absence of energy dissipation, a magnetic spin with magnetization $\mathbf{m}$ subject to an effective field $\mathbf{B}_{\text{eff}}$ will rotate around the effective field, and the angle between them will not change. However, in real systems there are sources for losses such as eddy currents, diffusion and reorientation of lattice defects [2]. These sources can be taken into account in computational methods by introducing the Gilbert damping parameter α, which allows $\mathbf{m}$ and $\mathbf{B}_{\text{eff}}$ to eventually align. This process is schematically presented in Fig. 2.1.

Magnetization of the DWs in PMA materials is in-plane, and depending on the rotation plane of the DW spins they are called either Bloch walls or Néel walls. In Néel walls the magnetization rotates in the normal plane of the DW, and in Bloch walls the magnetization rotates perpendicular to the normal plane of the DW [2]. The DW configuration that minimizes the energy of the system determines the equilibrium configuration of the DW magnetization. A schematic presentation of a Bloch wall is shown in Fig. 2.2a) and a Néel wall in Fig. 2.2b).

Magnetic DWs and their dynamics can be studied in several different ways. DWs can be seen as fractals [14], elastic lines [15] or topological defects that follow conservation rules of topology [16]. DW models can be used to study e.g. the Barkhausen effect, to which I will return in Section 2.5, including the power-law statistical description [17]. DWs can also be studied purely from engineering application point of view [5, 18, 19].

2.3 Walker breakdown

Field or current driven DW velocity v_{DW} as a function of field B_{ext} or current j tends to have two linear parts separated by an abrupt drop in velocity [20]. The drop is called Walker breakdown (WB), which is caused by the excitation of internal degrees of freedom in the domain wall magnetization $\mathbf{m}_{\text{DW}}$ [21] and it results in precessional DW motion. The abrupt average velocity drop is depicted

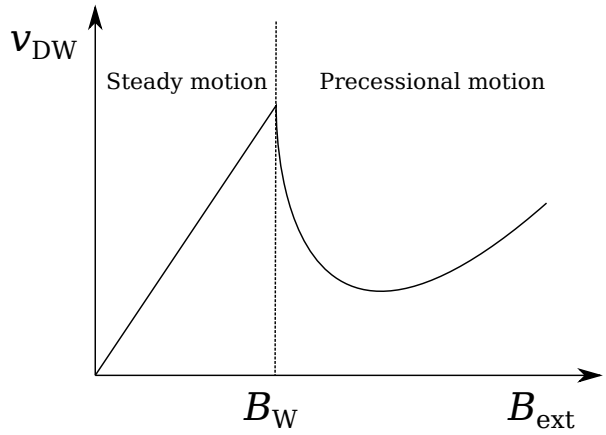

Figure 2.3. The average DW velocity v_{DW} drops abruptly if the applied field is increased above Walker field $B_{\mathrm{ext}} > B_{\mathrm{W}}$.

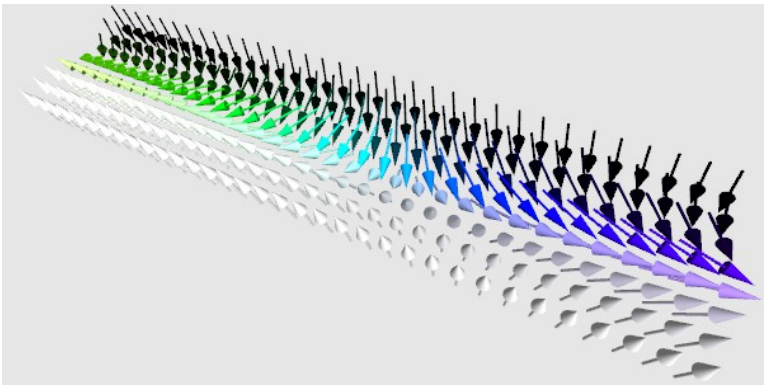

Figure 2.4. Schematic presentation of a tail-to-tail Bloch line.

in Fig. 2.3. When the applied field B_{ext} or current j is above Walker field B_{W} or current j_{W}, $\mathbf{m}_{\mathrm{DW}}$ starts to rotate as the DW moves. In 1D nanowires with PMA the rotation occurs as a periodic alternation between Bloch wall and Néel wall configuration. In the Néel wall phase, the DW moves momentarily backwards and proceeds forwards again when the magnetization rotates back to Bloch structure. As the field is further increased to $B_{\mathrm{ext}} \gg B_{\mathrm{W}}$ the rotation frequency increases and the DW velocity v_{DW} increases again linearly [10].

In soft magnetic nanowires, where the magnetization of the domains is in the material plane, the possible DW configurations are transverse wall, vortex wall and anti-vortex wall. Above B_{W}, the DW transforms periodically between transverse and vortex wall [10, 22].

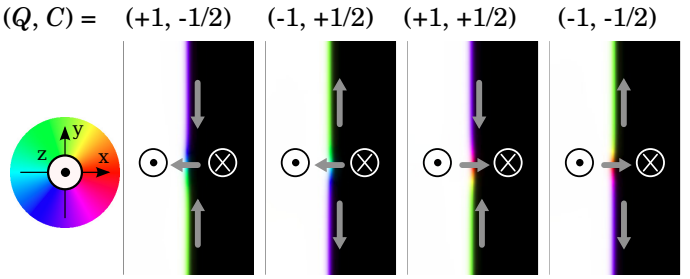

Figure 2.5. All four combinations of topological charge Q and chirality C for VBLs illustrated. Color wheel, arrows, in- and out-symbols depict the magnetization directions.

2.4 Bloch lines

The WB occurs in extended PMA nanostrips with longer DWs as well, but the mechanism is different. In these systems the WB takes place non-uniformly, i.e., we see "DWs within the DW". These local magnetization rotation regions within DWs are called Bloch lines (BLs) [23]. A schematic presentation of a vertical Bloch line (VBL) is shown in Fig. 2.4. The VBL is a Néel wall section separating two oppositely magnetized Bloch wall regions. The structure of the BL is formed across the thickness of the DW and is thus call a vertical Bloch line. The green and purple regions in the DW are opposite chiralities of the Bloch wall, which are separated by the cyan VBL-region. White and black areas correspond to $+z$- and $-z$-domains, respectively. The magnetization rotates by 180° along the DW across the VBL.

BLs were experimentally found in 1972–1976 in bubble domain structures [24]. BLs are topological defects within DWs, which are again topological defects within ferromagnets. BLs can be nucleated in films if DW dimensions are large relative to BL width $\Lambda = \sqrt{A/K_\mathrm{d}}$, where A is the exchange stiffness describing the strength of the exchange interaction, the stray field energy constant is $K_\mathrm{d} = M_\mathrm{S}^2\mu_0/2$ [24], and μ_0 is the vacuum permeability. VBL structures can be characterized by a topological charge $Q = \pm 1$ and chirality $C = \pm 1/2$ [16]. Here $Q = +1$ corresponds to head-to-head and $Q = -1$ to tail-to-tail spin configurations, and $C = 1/2$ corresponds to clockwise and $C = -1/2$ to counter-clockwise rotation of the spins within the DW when the inspection direction is fixed from bottom to top. The half-integer value of C is related to the 180° spin rotation. An illustration of the four degenerate states is presented in Fig. 2.5. Any of the configurations of BLs can be created on an edge or as a pair nucleation conserving the topological charge and chirality. All four degenerate states share the same energy level so their generation is equiprobable [2]. The type of nucleated pair or a generated BL is thus controlled by the driving field direction and magnetization of the DW. If a BL is generated in the center of the DW, they are always created in pairs. In pair generations and annihilations the topological charge will remain constant $\sum_i^{\text{before}} Q_i = \sum_i^{\text{after}} Q_i$ as well as chirality $\sum_i^{\text{before}} C_i = \sum_i^{\text{after}} C_i$. This is an example of a topological conservation law [25, 26].

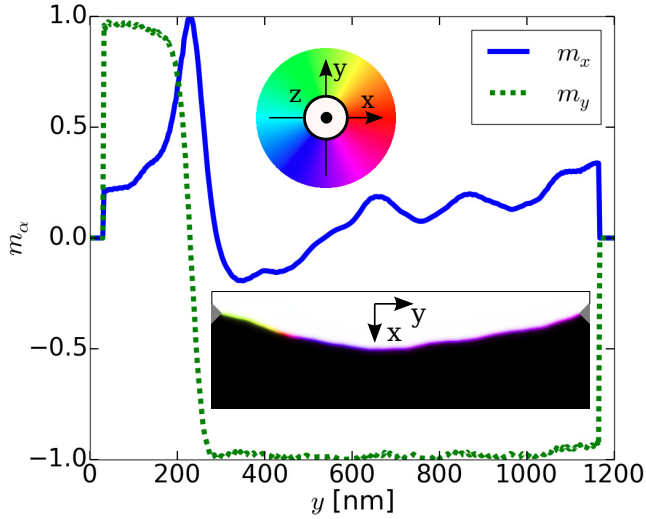

Figure 2.6. In-plane magnetization components m_x and m_y along a domain wall with a head-to-head Bloch line. A 2D view of magnetic structure is presented in the inset.

To further demonstrate the structure of a VBL the in-plane magnetization profile across a VBL is presented in Fig. 2.6 with a 2D view from the top of the sample in the inset. We can see how the DW magnetization component m_y changes sign across the VBL. At the center of the VBL $m_y = 0$ and $m_x = 1$.

Figs. 2.4, 2.5 and 2.6 concern a BL type that is called a vertical Bloch line (VBL). In thin films this is the only type of BL that can occur. However, if the sample thickness is increased, BLs can nucleate horizontally in the DW. This structure is called a horizontal Bloch line (HBL). The geometry of a HBL is presented in Fig. 2.7. HBLs can travel along up or down the DW and "punch through" at sample surfaces, which means that they unwind out of the system. These punch-through events are typically followed by a nucleation of another HBL [27, 28].

2.5 Barkhausen noise

Barkhausen noise was found in 1919 and is named after its finder Heinrich Barkhausen [29]. He noticed a crackling noise when he brought a permanent magnet in the proximity of a ferromagnetic object. Barkhausen believed that the noise is caused by a sudden reversal of an entire magnetic domain [17]. Several years later in 1938 W. Elmore discovered domain wall motion but he did not know it was related to Barkhausen noise [30]. Domain wall dynamics has since been studied intensively [31].

When a magnetic field **H** is applied to a ferromagnetic object the DW starts to

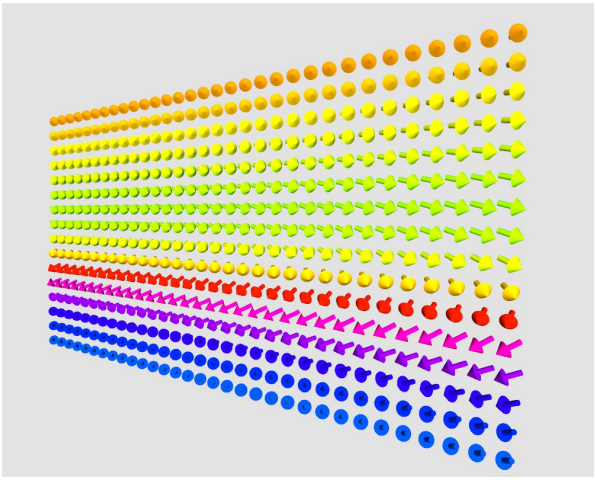

Figure 2.7. A schematic presentation of magnetization of a 2D DW with a HBL. The HBL-center is located at the red arrows pointing towards $+x$-direction. The $\pm z$-domains surrounding the DW are not shown, but the $+z$-domain is behind the shown DW and $-z$ in front of it. The magnetization near the surfaces is somewhat tilted towards Néel wall configuration and around the HBL they are close to Bloch wall configuration. Green color corresponds to $+y$-direction and purple to $-y$-direction.

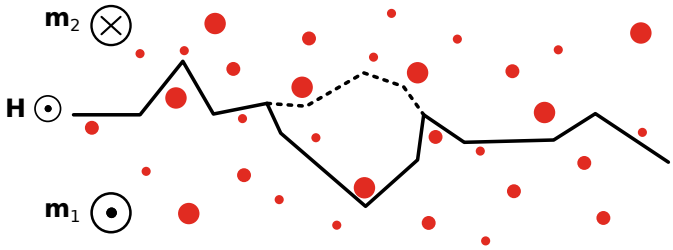

Figure 2.8. Schematic demonstration of the domain wall advancing with an avalanche after getting pinned by defects. Solid line is the domain wall before and the dashed line after the avalanche. The in and out symbols depict the magnetization directions in domains ($\mathbf{m}_1$ and $\mathbf{m}_2$), as well as the direction of the applied field $\mathbf{H}$. Red circles represent lattice defects.

propagate as the domains preferring the direction of **H** start to grow. DWs get pinned to defects in the magnetic media. The defects in crystalline materials consist for example of vacancies, non-magnetic impurities and dislocations. Eventually DWs unpin due to thermal effects or an increment of the applied field, and advance abruptly. These jumps are called avalanches [17]. A schematic presentation of a pinned DW advancing as an avalanche can be seen in Fig. 2.8.

Avalanche size is determined as $S = \int_0^T V(t)dt$, where T is the duration of the avalanche and $V(t)$ is the measured signal such as DW velocity. Avalanche is considered to be active during the time period with $V(t) > 0$, but in experiments the signal is rarely so perfect that it would go to zero. This is often overcome by using an artificial threshold value V^{th}, which is the limit where the avalanche crosses over between active and inactive state. Thus, the avalanche size is determined as

$$S = \int_0^T \left[V(t) - V^{\text{th}} \right] dt, \tag{2.1}$$

and the duration T is determined as the time period during which the condition $V(t) - V^{\text{th}} > 0$ holds. It is empirically observed and theoretically predicted that the avalanche size S and duration T distributions follow power laws with a cut-off [17]

$$P(S) = S^{-\tau_S} f(S/S^*), \tag{2.2}$$

and

$$P(T) = T^{-\tau_T} g(T/T^*), \tag{2.3}$$

where g and f are scaling functions, τ_S and τ_T are critical exponents, and S^* and T^* are cut-off values. The exponents do not depend on the underlying microstructure of the material but only on general symmetries, dimensionality and long-range properties of interactions of the material [17]. The statistics of the Barkhausen effect may also be discussed in the context of depinning of elastic manifolds in random media [17, 31]. Barkhausen noise can also be used to experimentally study if impurities or defects are present in a sample for non-destructive testing [32, 33].

2.6 Micromagnetics and MuMax3

The research in this dissertation was entirely conducted using micromagnetic simulations, which allows modeling a system with magnetic parameters of a realistic material. The basic work flow is to define geometry, number and dimensions of discretization cells, magnetic material parameters, apply field or current on the sample and study the system dynamics. One software that can do this task is MuMax3 [34]. It uses finite difference discretization of space and divides the defined sample into orthorhombic cells. MuMax3 is a GPU-accelerated micromagnetics software and has originally been developed at Ghent University but has now moved to community development [35].

Fundamentally micromagnetic simulations are based on integrating differential equations to determine how the magnetization evolves in space and time [34]. MuMax3 does it by solving the torque $\bar{\tau} = \partial \mathbf{m}/\partial t$, with contributions from three different torques: Landau-Lifshitz torque $\bar{\tau}_{\mathrm{LL}}$, Zhang-Li spin-transfer torque $\bar{\tau}_{\mathrm{ZL}}$ [36] and Slonczewski spin-transfer toque $\bar{\tau}_{\mathrm{SL}}$ [37]. The Landau-Lifhshitz torque can be formulated as [34]

$$\bar{\tau}_{\mathrm{LL}} = \gamma_{\mathrm{LL}} \frac{1}{1+\alpha^2} (\boldsymbol{m} \times \boldsymbol{B}_{\mathrm{eff}} + \alpha (\boldsymbol{m} \times (\boldsymbol{m} \times \boldsymbol{B}_{\mathrm{eff}}))), \tag{2.4}$$

where α is a damping parameter, $\boldsymbol{m} = \boldsymbol{M}/M_{\mathrm{S}}$ is the magnetization of a unit cell, which is dimensionless and has a length of 1. γ_{LL} is the gyromagnetic ratio and $\boldsymbol{B}_{\mathrm{eff}}$ the effective field, with contributions due to Heisenberg exchange, Zeeman, magneto-crystalline anisotropy and demagnetizing energies. Here I listed the relevant energies needed to understand the results of this dissertation. The spin-transfer torque terms are needed to take into account the effects of the current driven DW dynamics. It is possible to also study stability of magnetic structures by applying temperature, but usually the simulations are conducted in 0 K.

3. Bloch line dynamics in thin ferromagnetic strips

In this chapter I will discuss the effects of width of a thin ferromagnetic strip on DW dynamics. I will also discuss how BLs can be displaced within the DW by applying external magnetic field or spin polarized electric current. Further details on the matter can be found in Publication I.

3.1 Background

It is important to understand how the dynamics of DWs, including details such as the Walker breakdown, is affected by the sample geometry. Here I will focus on the role of the finite width of the strip. In nanowires the Walker breakdown proceeds via uniform rotation of the DW magnetization, but in extended strips the magnetization rotations become nonuniform and VBLs are nucleated. This research shows how the VBLs affect the DW velocity in different strip widths and VBLs can be nucleated and moved using in-plane fields or spin-polarized currents. We also show how VBLs could be nucleated within a DW pinned from the two ends due to notches at the strip edges to study their dynamics experimentally.

3.2 System

We simulate ferromagnetic CoPtCr strips with PMA. The thickness of the strip is $L_z = 20\,\text{nm}$, and widths L_y are ranging from 150 nm to $3\,\mu\text{m}$. The geometry is visualized in Fig. 3.1. The system length is fixed to $6\,\mu\text{m}$ and the simulation window is either fixed or moving along the DW depending on the simulation. Moving simulation window emulates an infinitely long strip.

Micromagnetic parameters for CoPtCr are exchange stiffness $A_{\text{ex}} = 10^{-11}\,\text{J/m}$, saturation magnetization $M_{\text{S}} = 3 \times 10^5\,\text{A/m}$, and the damping parameter $\alpha = 0.2$ [10]. Since CoPtCr is PMA material the easy axis is set to z-direction with the first order uniaxial anisotropy constant $K_{\text{u}} = 2 \times 10^5\,\text{J/m}^3$ [10]. The discretization of the simulation cells are $\Delta_x = \Delta_y = 3\,\text{nm}$ and $\Delta_z = 20\,\text{nm}$. We decided to use

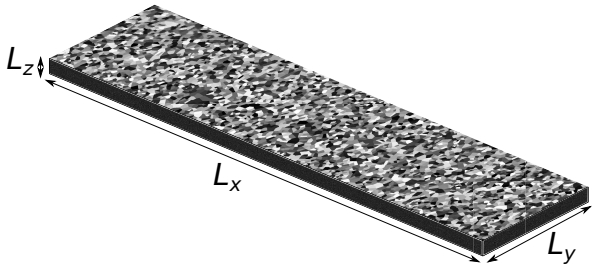

Figure 3.1. A schematic representation of a disordered sample material with the sample geometries length L_x, width L_y and thickness L_z depicted. Granular structure of the ferromagnetic strip is constructed using Voronoi tesselation.

only one layer of discretization cells in thickness, because in our tests we verified that the number of layers did not significantly affect the results.

The domain wall was initialized to a Bloch wall configuration with magnetization in the $+y$ direction. The configuration is similar as in the first panel ($t = 0\,\text{ns}$) of Fig. 3.4, although without the triangular notches at the top and the bottom.

We introduce disorder to the system by dividing the sample into grains by Voronoi tessellation with average grain size of 11.9 nm [38]. Each grain i is assigned with a varied uniaxial anisotropy constant $K_{\text{u,i}} = \mathcal{N}(K_\text{u}, \sigma^2)$, where σ is the standard deviation. Only the magnitude of uniaxial anisotropy is randomized and not the direction of the easy axis, which remains in the z direction.

3.3 Results

3.3.1 Field driven domain wall

We apply a constant field B_ext in $+z$ direction as shown in Fig. 3.2. The domain wall tilts slightly but notably counter-clockwise as can be seen in a narrow strip ($L_y = 150\,\text{nm}$) Fig. 3.2 (a) and in wider strip ($L_y = 1.2\,\mu\text{m}$) (c). We argue that this is caused by the applied field rotating the spins in the DW according to the first term of Eq. (2.4). Rotation of the DW spins generate magnetic charges on the two surfaces of the DW (it has a partial Néel wall character), which operate as sources of stray field. To minimize the stray field energy ($\mathscr{E}_\text{demag} = -\frac{1}{2}\mathbf{M}\cdot\mathbf{B}_\text{demag}$ [34]), the DW tends to align with the magnetization of the DW and causes the DW to tilt. Notice that the tilt occurs in the absence of Dzyaloshinskii-Moriya interaction [39]. When the field is increased above the Walker field $B_\text{ext} > B_\text{W}$, the internal degrees of freedom of the DW are excited. The magnetization of the DW of a narrow strip starts a close to spatially uniform counter-clockwise precession. The motion of the DW slows down, when the configuration of the DW is Néel-like. Fig. 3.2 (b) shows a snapshot of this precession, where the

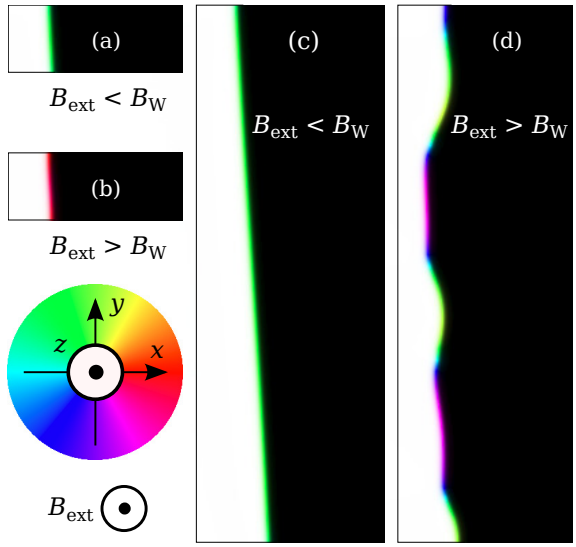

Figure 3.2. Snapshots of field driven DWs in a perfect narrow ($L_y = 150\,\text{nm}$) [(a) and (b)], and wider strip ($L_y = 1.2\,\mu\text{m}$) [(c) and (d)]. When the field is lower than Walker field $B_{ext} < B_W$, the DW propagates to $+x$ direction slightly tilted in both widths. When the field is increased to $B_{ext} > B_W$, the magnetization in the narrow strip starts close to uniform rotation (b). In wider strip the excitation of internal degrees of freedom become non-uniform and BLs are nucleated to the DW via pair nucleations and from the edges (d). Direction of the applied field is shown in the lower left corner. The color wheel depicts mapping between colors and magnetization directions. White is $+z$ and black is $-z$ direction.

magnetization of the domain wall is somewhere between $-y$ and $+x$. In the wider strip the excitation of the internal degrees of freedom become spatially non-uniform. This results in nucleation of BLs in the DW from the sample edges and also nucleation of BL pairs from inside of the sample. A very complex dynamics of nucleation and annihilation of BLs ensues. A snapshot of a wider strip with BLs is presented in Fig 3.2 (d).

To study the effect of disorder, we use $\sigma = 0.07K_u$ to achieve a depinning field $B_{dep} \approx B_W$. Results for the DW velocity $v_{DW}(B_{ext})$ for a perfect strip are presented in Fig. 3.3 (a), while the corresponding curve for the disordered system is shown in (b). In a perfect strip we see that B_W is around 10 mT, but with some variations depending on the system width L_y. We see that the magnitude of the abrupt velocity drop in the breakdown also depends on the strip width.

$v_{DW}(B_{ext})$ curves of the disordered system in Fig. 3.3 (b) look significantly different from the perfect system velocities. The narrow DWs seem to be more sensitive to the disorder and there the DWs seem to remain pinned for higher fields than in wider strips. This is an expected result as a longer DW drags pinned and retarding parts due to the elastic property of the DW. When the DW is narrowed to the limit of 0D, it will not benefit from such drag effects and will be more likely get pinned to the disorder. Furthermore, the breakdown seems to

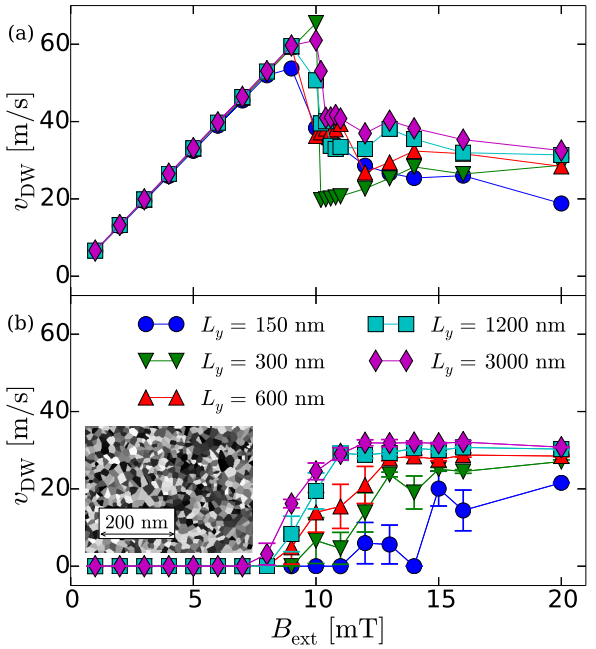

Figure 3.3. Domain wall velocity v_{DW} as a function of B_{ext} in perfect strips (a) and in disordered strips (b) with random anisotropy in each grain ($\sigma = 0.07K_{\mathrm{u}}$). The inset depicts the simulated granular structure using Voronoi tessellation with average grain diameter of 11.9 nm.

happen with a lower field for the disordered system than for the perfect strip. In fact, all the moving DWs experience Walker breakdown in the sense that BLs are nucleated within the DW. This is due to the way the disorder is implemented. With the local variations of uniaxial anisotropy the BL nucleation process can start at lower fields than in a perfect system. Even applied constant fields exceeding B_{dep} sometimes results in the DW getting pinned by the disorder.

3.3.2 Bloch line generation

We want to demonstrate a method for possible experiment, where DW is spatially confined and the BLs are generated within the DW. This method could be used for studying BL dynamics, which will be demonstrated in Section 3.3.3. We construct a geometry to pin DWs from the edges and increase the magnitude of the disorder to $\sigma = 0.1K_{\mathrm{u}}$ to ensure pinning of the DW to the grains. The design is then used to study BL dynamics. Implemented triangular notches (50-nm-long sides and $50\sqrt{2} \approx 70.2$-nm-long base) for DW edge pinning are shown in Fig. 3.4 in gray. The strip width is $L_y = 1.2\,\mu$m and length is $L_x = 6\,\mu$m.

First we apply ± 20 mT field pulse to z-direction for 5 ns. Then we let the system to relax for 19 ns. The high field starts to curve the DW and generate BLs to the DW while the edges remain pinned to notches. Complex dynamics

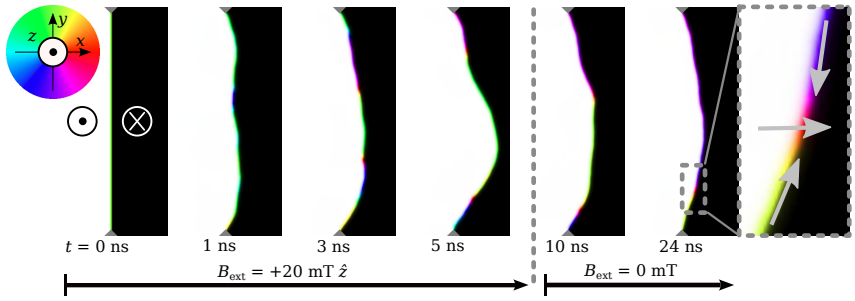

Figure 3.4. Bloch line generation with a 5 ns field pulse of $B_{\text{ext}} = 20$ mT $> B_{\text{W}}$ magnitude. After the pulse the system is let to relax for 19 ns. In this example two pairs of BLs are nucleated in the DW during the pulse and 3 of the BLs unwind on the edges leaving one H2H BL with $\mathbf{m}^{\text{BL}} = +\hat{\mathbf{x}}$. The BL is shown magnified in the last frame. The colorwheel depicts the color to magnetization direction mapping.

occurs during the field pulse including pair nucleations and annihilations, and unwinding of BLs on the DW edges. After the field pulse, the DW and the BLs it may contain get pinned by the disorder.

From a total of 100 disorder realizations roughly 40 % succeeded to generate a single stable 180° BL within the pinned DW. The probability of the remaining single BL configuration to be head-to-head (H2H, $Q = +1$) or tail-to-tail (T2T, $Q = -1$) did not depend on the direction of the field pulse and they were generated equally likely. The remaining 60 % that did not result into a single BL include multiple BLs, 360° BLs or no remaining BLs in the relaxed state. It is much more probable to nucleate a BL with $m_x^{\text{BL}} < 0$ using $-z$ field, and the other way around for $+z$ field. Thus, a $+z$ field was used to generate BLs with magnetization $m_x^{\text{BL}} > 0$ and the DWs are bending to the $+x$ direction in Fig. 3.5 (a) and (c), and a $-z$ field generated $m_x^{\text{BL}} < 0$ BLs with the DWs bending to the $-x$ direction in (b) and (d).

3.3.3 Field driven Bloch lines

We collect an ensemble of DW configurations with a single BL with all four permutations of the topology generated with the method discussed in the previous section. Different configurations are presented in Fig. 3.5 showing only the x-component of the magnetization in gray scale. Topologically it is possible to have a single BL if the system has open boundary conditions. BLs can be only generated in pairs if the system is infinite or has periodic boundary conditions. After a field pulse followed by a relaxation period consisting a complex process of nucleation and annihilation of pairs, winding and unwinding of isolated BLs from the edges, a single BL remaining within the DW is driven with $\pm y$ field to the lower edge of the DW.

The structure of the BL determines the direction of the applied field needed to move it. Field to $+y$-direction drives a H2H BL to $+y$-direction and $-y$ field drives it to $-y$-direction, and vice versa for a T2T BL.

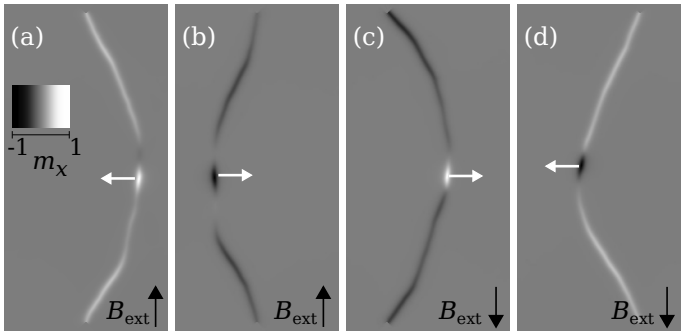

Figure 3.5. Snapshots of BLs driven from bottom to top with an applied in-plane field. All possible configurations are H2H (a) and (b), and T2T (c) and (d) with $\mathbf{m}^{\text{BL}} = \pm\hat{\mathbf{x}}$ The direction of the applied field is depicted with the black arrows. The grayscale of the image shows the magnitude of $\mathbf{m}_{\mathbf{x}}$. The white arrows show the direction of the force on the DW induced by the applied field acting on the BL.

The white arrows in Fig. 3.5 present the direction of the force induced by the applied field acting on the BLs. The force originates from the first term of Eq. (2.4). The in-plane field rotates the BL magnetization to the direction of either $+z$ or $-z$ growing the corresponding domain, which results in a local force acting on the DW at the location of the BL. Another force acting on the domain wall is the line tension originating from the property of the domain wall trying to minimize domain wall energy, which is achieved by minimizing the length of the DW. The competition between these forces determine how the DW behaves as a BL is travelling along it.

The BLs are driven along the curved DWs. The results for velocities averaged over 5 disorder realizations for all 4 possible configurations are presented in Fig. 3.6. The velocities of BLs with corresponding configurations in perfect and straight DW are presented with 4 stacked solid black lines. v_{BL} is indistinguishable between the different configurations in perfect strip with a straight DW. From these results it seems that in disordered films H2H BLs move slower than T2T and slower than in perfect strip.

The curvature seems to be boosting the BL propagation velocity. Analysis of the animations reveals that the H2H-BL bends and reconfigures the DW shape as the BL travels along the DW. The reshaping of the DW momentarily pushes the BL backwards which effectively drops the average velocity v_{BL}. This seem to happen less in T2T configured BLs because the BL induced force is acting on the opposite direction than the line tension. This can be seen in Figs. 3.5(c) and (d).

3.3.4 Current driven Bloch lines

We construct an academic demonstration of a possible memory application based on BLs. We concider a CoPtCr strip with $L_x = 90\,\text{nm}$ depicted in the inset of Fig. 3.7. The spin polarized current of magnitude j_{ext} is conducted in the strip to $-y$-direction (conduction electrons moving to the $+y$-direction).

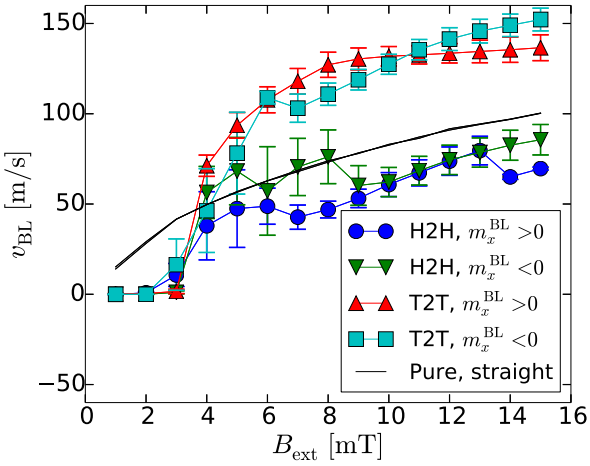

Figure 3.6. Bloch line velocities driven with applied field. All the possible BL magnetization confiugrations are measured and the results are averaged over 5 realizations of the initialized BL generations. Head-to-head (H2H) and tail-to-tail (T2T) with BL magnetization $m_x^{\mathrm{BL}} = \pm\hat{\mathbf{x}}$. The BL velocities with the corresponding configurations in perfect strip with straight DW are presented with stacked 4 solid black lines.

A single BL travels along the DW seemingly in the same way as a BL driven with an applied field though the mechanism is quite different [3]. A BL is moved to the direction of conducting electrons by the spin transfer torque. When current-carrying electrons hit a BL, the magnetic moment is transferred from the previous magnetic structure to the interface causing torque to it. The transfer of the moment effectively moves the BL unchanged to the traveling direction of the electrons. The mechanism is also used to operate the magnetic racetrack memories [5].

The dependence of the BL velocity on the applied current density in a straight DW driven with spin polarized current is presented in Fig. 3.7 with different nonadiabatic parameter ξ values. We consider $\xi = 0$, $\xi = \alpha = 0.2$ and $\xi = 2\alpha = 0.4$. With $\xi = 0$ the BL remains intrinsically pinned while for $\xi = 0.4$, we observe velocities as high as $v_{\mathrm{BL}} = 490\,\mathrm{m/s}$.

3.4 Discussion

The finding of high achievable BL velocities for both current and field driven BLs suggest that the BL based technology could be in principle employed for spintronics applications such as BL memories. The BLs do not experience breakdown due to the topological protection of the surrounding magnetic domains and conservation of topological charge and chirality, which would improve the predictability of the operation of hypothetical BL based devices. Also the significance of BL dynamics on DW propagation had been largely neglected in the recent literature before our Publication I came out. A year after its publication an interesting

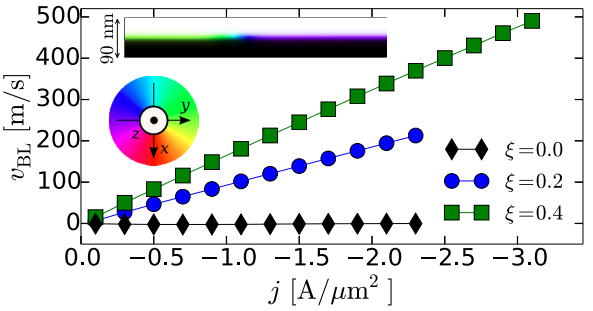

Figure 3.7. Current driven v_{BL} as a function of the current density j in a straight domain wall with a different values of nonadiabatic parameter ξ. The inset shows the strip width and driven BL-configuration. For $|j|$ values greater than the ones shown in the figure break down the domain structure.

study on the energy dissipations originating from VBL annihilations affecting the DW dynamics was done by Voto *et al.* [40] and another by Yoshimura *et al.* [16].

A study focusing on BLs driven with an in-plane magnetic field in 7.5 μm thick garnets with straight DWs was done by Logginov *et al.* [41]. Their results for $v_{\mathrm{BL}}(B_{\mathrm{ext}})$ show some similarities with our results for BL velocities in disordered media with curved DWs. There is a region of high BL mobility ($\mu_{\mathrm{BL}} = dv_{\mathrm{BL}}/dB_{\mathrm{ext}}$) at low fields followed by a $v_{\mathrm{BL}}(B_{\mathrm{ext}})$ saturation. But to our knowledge, an experiment with a stationary DW and the BL displacement being directly controlled using spin polarized electric current has not been done. Here we have shown its feasibility in theory. Our demonstration of the current driven BL setup is a bit problematic though. The construction of a system, where a long DW is confined in the center of a narrow magnetic strip, may be extremely difficult to execute in practice. Designing the experimental system and measurements to study current-driven BL dynamics would be an interesting path for future research. This research shows that BLs play important role in DW dynamics and that also the dynamics of the BLs themselves are worth studying.

4. Bloch lines in 3D garnets

In this chapter I will extend the research of BLs from 2D to a 3D system with PMA. BLs have more complex structure in 3D as they become actual lines spanning across the 2D DW. I will discuss the dynamics of DWs in systems with periodic boundary conditions (PBCs) as well as open boundary conditions (OBCs). This chapter is based on the published article in Publication II.

4.1 Background

DW dynamics has been widely studied in bulk materials, yet the internal evolution of the magnetization the DW experiences during its motion is not well understood. The magnetization inside the material can be hard to measure experimentally, as the DW is constantly moving, the surface might be non-transparent and the process can be relatively fast. The software and computation power has developed during the recent years to make it possible to visualize magnetization even in macroscopic systems [42]. There are materials, where the measurement of the DW magnetization within a bulk material is possible but they are limited to optically transparent materials [2]. To study the DW dynamics in 3D structures we wanted a material that can be grown arbitrarily thick such that it still maintains its uniaxial anisotropy. We decided to use a magnetic garnet that fulfills this requirement, since it can be epitaxially grown on a substrate inducing a crystalline PMA [24].

4.2 System

The simulated material is the magnetic garnet $(GdTmPrBi)_3Fe(Ga)_5O_{12}$ with saturation magnetization $M_S = 8992\,A/m$, exchange stiffness $A_{ex} = 2.2\times10^{-12}\,J/m$, uniaxial out-of-plane anisotropy $K_u = 602.5\,J/m^3$ with $\pm z$ easy axis, and damping parameter $\alpha = 0.15$ [43]. The quality factor of this material $Q = K_u/K_d = 11.9$, where the stray field energy constant is $K_d = M_S^2\mu_0/2 \approx 50.8\,J/m^3$, and μ_0 is the vacuum permeability. The Bloch wall width parameter is $\Delta = \sqrt{A/K_u} \approx 60\,nm$.

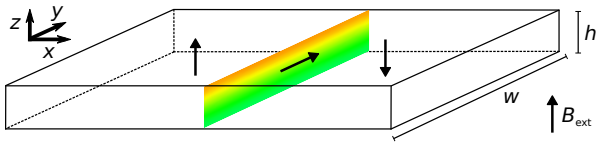

Figure 4.1. Schematic presentation of the initial magnetization of a relaxed domain wall in $h = 990\,\text{nm}$ strip ($B_{\text{ext}} = 0$). The magnetization of domain wall and the domains are visualized with color-coding shown in the color wheel and with arrows as well. The $\pm z$ domains surrounding the domain wall generate a demagnetizing field, which turns the magnetization roughly by $\pm 37^\circ$ on the top and bottom surface (orange and darker green, respectively) from the pure $+y$ Bloch wall (light green) in the center $z = h/2$.

The width of the sample is fixed to $w = 3.84\,\mu\text{m}$ and the moving simulation window is of length $30.72\,\mu\text{m}$. The simulation window is centered such that the average x position of the DW is kept within one simulation cell from the window center. The thickness h is varied between $h = 30$ nm and $h = 1.89\ \mu m$.

The magnetization is initialized to $+z$ and $-z$ domains separated by $+y$ Bloch wall and let to relax into its equilibrium configuration. A schematic presentation of the computed DW magnetization of a relaxed DW is shown in Fig. 4.1 . The arrows and color coding represent the magnetization directions in the DW.

The domains generate magnetic surface charges, which induce demagnetizing fields near the surfaces. Due to the flux closure tendency in magnetic systems the demagnetizing field tends to tilt the DW magnetization towards a Néel structure in the static case with $B_{\text{ext}} = 0$ [24, 44]. Close to the sample surfaces critical points $z_a(h)$ and $z_b(h)$ can be defined, where Bloch lines are nucleated [23]. For a static isolated DW the demagnetizing field acting on the DW is $H_{\text{S}}(z) = 4M_{\text{S}} \ln[z/(h-z)]$ in the limit $\Delta/h = 0$ [23] with the sample surfaces at $z = \{0, h\}$. The critical points are where $|H_{\text{S}}| = 8M_{\text{S}}$, which results to $z_a(h) = h/\left(1+e^2\right)$ and $z_b(h) = he^2/\left(1+e^2\right)$ [23]. At the critical points the balance of exchange interaction and stray field leaves the spins of the DW most labile. The twist of the domain wall is suppressed by exchange stiffness for thin films [2].

4.3 Results

In this section I will present our results for DW propagation velocities and study the non-monotonic dependence of the local maximum velocity of the DW on the strip thickness with both PBCs and OBCs. Different boundary conditions affect the BL nucleation mechanism in thin and intermediate thicknesses. In this chapter I refer to average DW propagation velocity as $v \equiv v_{\text{DW}}$.

4.3.1 Periodic boundary conditions

First we start by considering PBCs in the y direction. The DW propagation velocity v as a function of sample thickness h and external field B_{ext} are presented

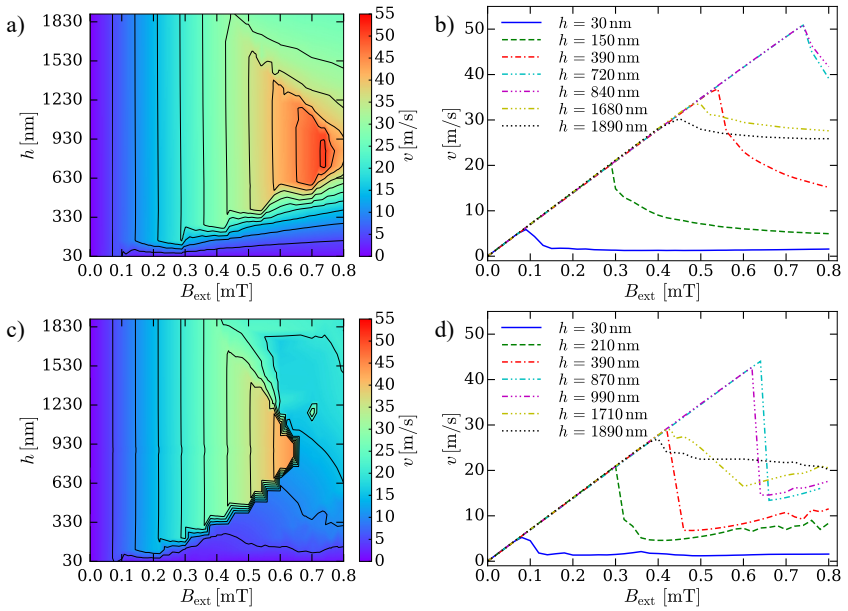

Figure 4.2. Average domain wall propagation velocity $v(h,B_{\text{ext}})$ to x direction for PBCs in (a) and (b); and for OBCs in (c) and (d). The velocity is determined from a linear fit to $x(t)$ excluding an initial transient. With $B_{\text{ext}} > B_{\text{ext}}^{\max}(h)$, the fit it done to the $x(t)$ signal after the moment the average y component of magnetization changes sign. A fixed 100 ns transient is used for $B_{\text{ext}} < B_{\text{ext}}^{\max}(h)$. The contour lines in (a) and (c) correspond to 5 m/s difference in velocity.

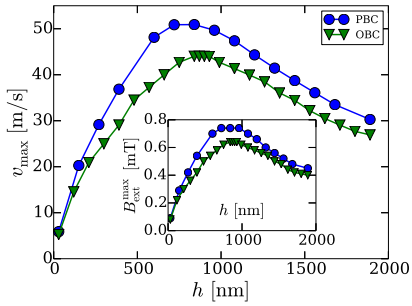

Figure 4.3. Maximum DW propagation velocity $v_{\max}(h)$ is derived from Fig. 4.2 as the last point on the linear part of the velocity curves. Corresponding driving fields $B_{\text{ext}}^{\max}(h)$ are presented in the inset.

in Fig. 4.2 (a) and (b). It can be seen that $v(B_{\text{ext}})$ is linear below a h-dependent threshold velocity. Within this region the DW magnetization remains constant during the DW progression and the mobility $\mu = dv/dB_{\text{ext}}$ of the DW follows a well known theoretical result for steady DW motion $\mu_{\text{steady}} = \gamma\Delta/\alpha \approx 71\,\text{ms}^{-1}\text{T}^{-1}$ for all h [24].

The h-dependent peak DW propagation velocity v_{max} is presented in Fig. 4.3 with blue circles. The data is extracted from Fig. 4.2 as the local maximum velocity w.r.t. h. Corresponding threshold fields $B_{\text{ext}}^{\text{max}}$ are reported in the inset of Fig. 4.3. Both curves show interesting non-monotonic character. To understand this behavior, we need to consider the modes of excitations allowed by the edges of the sample and how they depend on h.

In thin samples with $h \leq 150\,\text{nm}$, we observe close to uniform rotation of the magnetization similarly to Walker breakdown dynamics observed in nanowire geometries. The magnetization does not rotate with constant rate. B_{ext} slowly rotates the domain wall magnetization $\mathbf{m}_{\text{DW}}$ from pure Bloch structure towards Néel structure followed by an abrupt rotation to oppositely magnetized Bloch wall structure, where the rotation is slowed down again. Also, during the Néel phase v is decreased compared to Bloch phase.

When h is increased to "intermediate" thicknesses ($150 < h < 720$ nm), we start to see some internal structure developing in the DW magnetization with applied field greater than threshold field $B_{\text{ext}}^{\text{max}}$. A HBL with rotation less than π radians is generated near a surface moving towards the other surface. When the HBL reaches the opposite surface, it punches through and immediately a HBL with opposite magnetization is generated. The magnetization of the HBL and DW determine the direction of the travel. If magnetization above the HBL is $+y$, $-y$ below and $m_x^{\text{BL}} = +1$, the HBL travels to $-z$ direction or if $m_x^{\text{BL}} = -1$, the HBL travels to $+z$ direction. If the Bloch wall regions around the HBL are swapped, the travel directions are the other way around. Due to our initialization and the driving field applied always in the $+z$ direction we always nucleate the HBL at the bottom surface with $m_x^{\text{BL}} = -1$. In general the chirality controls the HBL travel direction according to Eq. (2.4).

If the thickness is further increased we start to see a "full" π HBL nucleate and propagate up and down the DW as shown in Fig. 4.4, where $h = 1.89\,\mu\text{m}$ and $B_{\text{ext}} = 0.6\,\text{mT}$. Figure 4.4 (a) shows a HBL about to punch through at the top surface of the sample followed by the nucleation of an oppositely magnetized HBL traveling towards the bottom surface ($-z$ direction) of the sample. In Fig. 4.4 (b) the HBL nucleated at the top surface has almost reached the bottom and will punch through at the bottom surface.

Understanding the nonmonotonic h-dependence of v_{max} and consequently B_{max} I want to point out two theoretical result and one conclusion of our own. Based on the theoretical calculations by Slonczewski and Malozemoff [24, 23] the maximum velocity $v_{\text{max}} \sim 1/h$ when the thickness h is greater than the so-called Bloch line limit, i.e. $h \gg \Lambda = \sqrt{A/K_{\text{d}}} \approx 208\,\text{nm}$. Similar behavior can be seen in our results in Fig. 4.3.

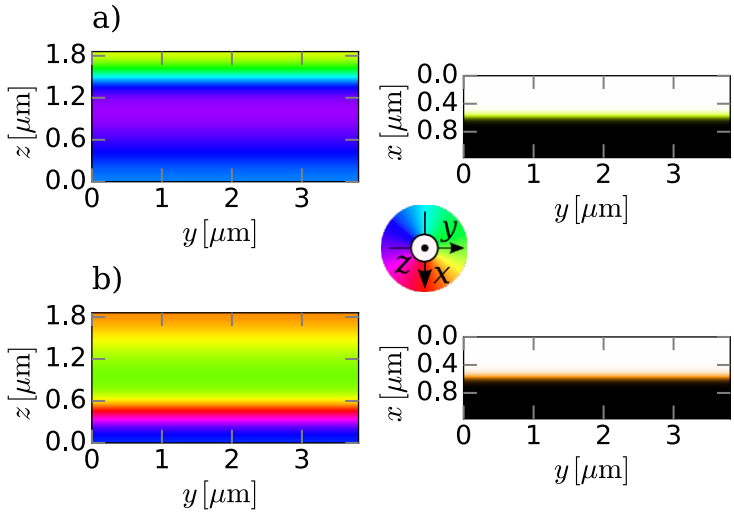

Figure 4.4. Snapshots of magnetization configurations of the domain wall with PBC in the y direction under $B_{\text{ext}} = 0.6\,\text{mT}$ in a strip with $1.89\,\mu\text{m}$ thickness. Left panel shows the DW magnetization viewed from $+x$ direction. The right panel shows magnetization from the top of the sample as it would be seen if it was experimentally measured. In (a) a HBL with magnetization $m_x^{\text{BL}} = -1$ (cyan color) is propagating to $+z$ direction and is about to punch through on the top surface of the sample. The punch through is shortly followed by a nucleation of another HBL with opposite magnetization. As can be seen from the right panel, the DW would seem like a normal Bloch wall if it was magneto-optically imaged. In (b) a HBL with magnetization $m_x^{\text{BL}} = +1$ (red color) is travelling to $-z$ direction and is about to punch through from the bottom surface. The color wheel shows the mapping between colors and the direction of the in-plane magnetization, and white and black correspond to $+z$ and $-z$ magnetizations, respectively.

For the thin strips this does not apply, because the DW exhibits a spatially uniform rotation of magnetization and there is no space for a HBL. Instead one may apply the theory by Mougin *et al.* [20], which assumes that the Walker field in confined geometries takes the form of $H_W = 2\pi\alpha M_S|N_x - N_y|$, where N_x and N_y are the demagnetizing factors along x and y, respectively. Since we have PBCs in y, $N_y = 0$ and using the elliptical approximation for N_x [20], we obtain $H_W = (2\pi\alpha M_S h)/(h + \Delta)$ and $v_{max} = (2\pi\gamma\Delta M_S h)/(h + \Delta)$. These results are in qualitative agreement with our results in Fig. 4.3.

The two regimes, which follow the theories, are separated by a region with the maximum of v_{max}. In our system the maximum is at $h \approx 840\,\text{nm}$. This h roughly coincides with $z_a(h) + [h - z_b(h)] + \pi\Lambda \approx 850\,\text{nm}$, where $z_a(h)$ and $z_b(h)$ are the critical points, and $\pi\Lambda$ is the natural BL width [24]. It seems that when h is great enough to accommodate a full HBL in addition to the critical points, the energy barrier to nucleate HBL becomes lower and v_{max} starts decreasing.

4.3.2 Open boundary conditions

Next we consider the same system with OBCs to understand how the edge effects alter the dynamics of the DW. Average velocities $v(B_{ext}, h)$ are reported in Figs. 4.2(c) and 4.2(d). The linear part is the same as for PBCs, but the maximum velocity is reached with lower field values than with PBCs. The velocity drop with field greater than the threshold field B_{ext}^{max} is also more abrupt for OBCs than for PBCs. In Fig. 4.3 v_{max} is marked with green triangles, and it shows the same results. The differences between OBCs and PBCs can be reasoned to be caused by the edges enabling more ways to nucleate BLs. The theoretical origin for this difference may be concluded from the aforementioned theory of Mougin *et al.* [20], where in the case of OBCs $N_y \neq 0$, which lowers the Walker field H_W and thus v_{max} as well. In the thickest systems and in particular in the $h = 1.89\,\mu\text{m}$ sample v_{max} and B_{ext}^{max} (Fig. 4.3) and the nature of the DW dynamics become very similar for OBCs and PBCs, but the punch-through event is different. In the OBC system the punch-through occurs in a way where the HBL ends both get to the surface, approach each other and annihilate. This is immediately followed by nucleation of another HBL, traveling to the opposite direction.

In thin systems with $h \leq 210\,\text{nm}$, we observe a subsequent nucleation of typical VBLs traveling from one edge to the other. The Bloch lines are similar to the ones discussed in Chapter 3. Fig. 4.5a) shows a snapshot of a tail-to-tail VBL traveling to $+y$ direction in a $h = 210\,\text{nm}$ sample. In slightly thicker systems $210\,\text{nm} < h < 390\,\text{nm}$ we observe VBLs traveling back and forth between the edges. In this thickness range we also start to see the slight deformation of the VBL due to the demagnetizing field originating from the surface charges. The demagnetizing field is pointing to $+x$ direction on the top surface and to $-x$ direction on the bottom surface. This breaks the symmetry between the surfaces and deforms the magnetization of a VBL.

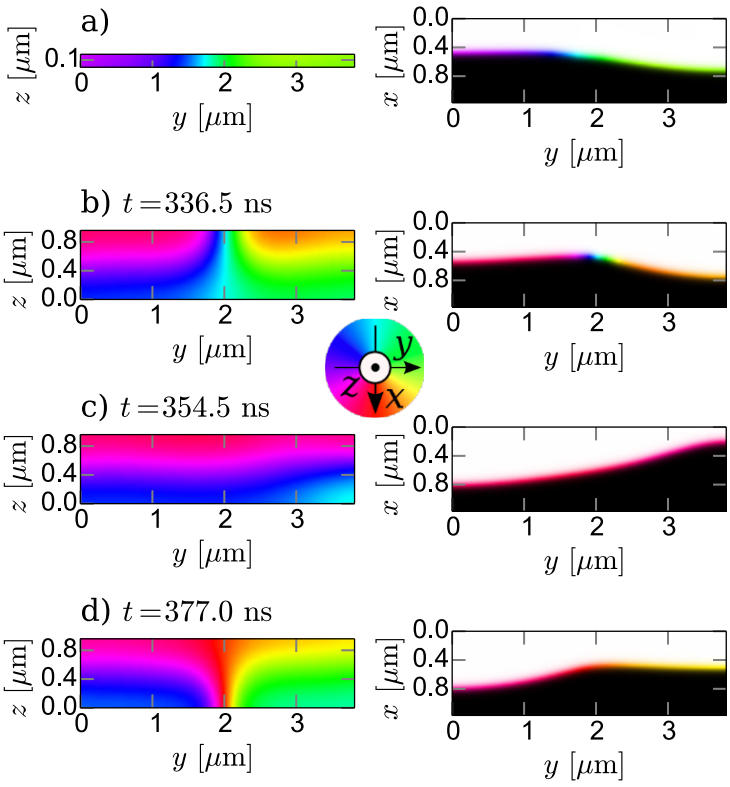

Figure 4.5. Snapshots of the DW magnetization with OBCs in the y direction. The left panel shows the magnetization within the DW, where the DW position is defined as $m_z = 0$. Right panel shows the magnetization on the top face of the sample. The DW position is defined as $m_z = 0$. (a) shows a snapshot of magnetization profiles for a strip of thickness $h = 210\,\text{nm}$, and field $B_{\text{ext}} = 0.32\,\text{mT}$. A VBL is traveling to $+y$ direction. Figures (b), (c) and (d) are snapshot from strip with thickness $h = 990\,\text{nm}$ and $B_{\text{ext}} = 0.64\,\text{mT}$. A deformed $-x$ (cyan color) VBL is traveling to $+y$ direction along the top face of the sample in (b). After reaching the edge, the VBL transforms into HBL in (c) and travels to the bottom face and transforms back to VBL in (d) with $+x$ magnetization (red color). The VBL with $+x$ magnetization travels $-y$ direction and $-x$ to $+y$ direction due to the direction of the applied field. Notice how the VBL is hardly visible from top view apart from the retarded region in the domain wall. The color wheel shows the mapping between colors and the direction of the in-plane magnetization, and white and black correspond to $+z$ and $-z$ magnetizations, respectively.

Further increasing the thickness of the sample ($390\,\text{nm} \leq h < 1.26\,\mu\text{m}$) makes the VBL deformation more pronounced. Snapshots of a BL dynamics in $h = 990\,\text{nm}$ sample are presented in Figs. 4.5(b), 4.5(c) and 4.5(d). The figures show how a VBL is traveling along the top surface to $+y$ direction in Fig. 4.5(b). The deformation of the VBL is evident here. The magnetization rotates roughly 2π on the top surface (seen also in the right panel) and only about $\pi/2$ at the bottom surface. When the VBL reaches an edge it transforms into a short-lived partial HBL structure with rotation less than π [4.5(c)], and it travels to $-z$ direction. When the edge of the HBL reaches the bottom surface of the sample it transforms back into a VBL and travels to the $-y$ direction [4.5(d)]. The full Bloch line cycle takes approximately 83 ns determined from the system in Figs. 4.5(b), 4.5(c) and 4.5(d), and the deformed VBL travels across a face of the sample in 31 ns. This results in velocity ratio $\kappa = v_{\text{BL}}/v_{\text{DW}} \approx 8.5$, which is relatively close to the experimental result $\kappa \approx 10.2$ by Thiaville *et al.* [43] for the material we consider here. We measure κ values in the range of 8–12 for systems where VBLs occur. Dynamics of these deformed VBLs have been previously studied in [43, 45, 46], but to our knowledge the circulation of a Bloch line has not been reported before.

OBCs have a transition region in the thickness range $1.26\,\mu\text{m} \leq h \leq 1.71\,\mu\text{m}$, where the internal activity starts as a few HBL punch through events followed by a transition to the VBL circulation dynamics. In other words, both of the aforementioned dynamics occur in the same system. The DW velocity $v(t)$ has two phases as well. The DW is moving forward with constant velocity during the HBL propagation, but during the punch through the DW stops and travels backwards (approximately for 1 ns), and then proceeds forwards after nucleation of a new HBL. In VBL phase the DW is constantly moving forwards with slight oscillation of $v(t)$. In this thickness region the abrupt velocity drop with $B_{\text{ext}} \gtrsim B_{\text{ext}}^{\text{max}}$ is smoothed out in Fig. 4.2(c) and 4.2(d). For instance for $h = 1.71\,\mu\text{m}$ and $B_{\text{ext}} = 0.7\,\text{mT}$ the average DW velocity is $\sim 5\,\text{m/s}$ higher for HBL phase than for the VBL phase. In Fig. 4.2 we always report the steady state velocity after any initial transient.

Finally an anomaly at $h = 1.17\,\mu\text{m}$ and $B_{\text{ext}} = 0.7$ mT should be noted. It can be seen as a small island of faster average velocity in the ocean of the slower velocity in Fig. 4.2(c). At this specific point the DW shows purely HBL-based dynamics, while in the region around it, the DWs show the VBL dynamics. This could be explained by the relative shortness of the simulation time and the DW may not have reached its steady state. We verified the results with $B_{\text{ext}} = \pm\epsilon$, where $\epsilon = 0.001$ mT, with the same results.

4.4 Discussion

In this chapter I discussed the Bloch line dynamics in garnet films of various thicknesses. We reported a non-monotonic dependency of maximum velocity with

stable motion $v_{\max}(h)$ w.r.t. h. We linked our results to theories by Mougin *et al.*[20] for thin systems and to the theory by Slonczewski and Malozemoff [23, 24] for thicker systems. We noticed that the maximum of $v_{\max}(h)$ is roughly where h can accommodate a HBL in addition to the critical points where the HBLs are generated. The difference in $v_{\max}$ between PBCs and OBCs is related to the lower energy barrier needed for VBL nucleation, but the differences diminish as the system thickness is increased. To our knowledge, 3D simulations for this size scale have never been conducted using micromagnetic approach.

We also report the circulation of a BL around the perimeter of the DW, which has not been reported before. This is probably due to the limitations of imaging techniques and excessive amount of computational resources needed for these simulations. The optical imaging techniques can observe the magnetization through a transparent sample [2]. If the observation is limited to the surface of the sample, we suggest that scanning transmission x-ray microscopy (STXM) would provide the needed spatial and temporal resolution for the purpose [47]. It would be interesting to find experimental verification of our results of the internal dynamics of DWs. As the right panels in Figs. 4.4 and 4.5 show, the magnetization of the DW experimentally measured with e.g. a magneto-optical method, may only show rotation of $\pi/2$ radians at the surface when the part of VBL with more spin rotation is at the bottom surface. Neglecting such details could lead to false interpretations of the dynamics.

5. Barkhausen noise from precessional domain wall motion

In this chapter I will take a completely new angle to DW dynamics by studying the Barkhausen effect in thin magnetic films with PMA using micromagnetic simulations. The DWs that experience a Walker breakdown nucleate VBLs and the statistics of the avalanches of VBLs are studied in parallel with the traditional DW movement related to the Barkhausen effect. This chapter is based on the unpublished article in Publication III.

5.1 Background

Vast amount of numerical and experimental research has been conducted on the Barkhausen effect [17], but it has not been studied using micromagnetic simulations due to the demand for large amount of statistics and computational power needed to run the simulations. Recently there has been some related research employing the micromagnetic approach, but it has focused on the depinning phase transition [48, 49]. Our aim is to compare the classical way of analyzing the avalanche statistics from DW velocity to the magnetization activity bursts seen in the internal DW magnetization caused by the dynamics of VBLs during avalanches.

5.2 System and methods

We simulate a Pt/Co/Pt multilayer system with a 0.5 nm thick Co film with perpendicular magnetic anisotropy. The material parameters experimentally determined by Metaxas *et al.* [50] are exchange stiffness $A_{\mathrm{ex}} = 1.4 \times 10^{-11}$ J/m, saturation magnetization $M_{\mathrm{S}} = 9.1 \times 10^5$ A/m, uniaxial anisotropy $K_{\mathrm{u}} = 8.4 \times 10^5$ J/m^3, and the damping parameter $\alpha = 0.27$. The domain wall width parameter is $\Delta_{\mathrm{DW}} = \sqrt{A_{\mathrm{ex}}/K_0} \approx 7$ nm, where $K_0 = K_{\mathrm{u}} - \frac{1}{2}\mu_0 M_{\mathrm{S}}^2$ is the effective anisotropy. The film length, width and thickness are $L_x = 1024$ nm, $L_y = 4096$ nm and $L_z = 0.5$ nm, respectively. The moving simulation window algorithm differs from original implementation in MuMax3, such that the center of the simulation window

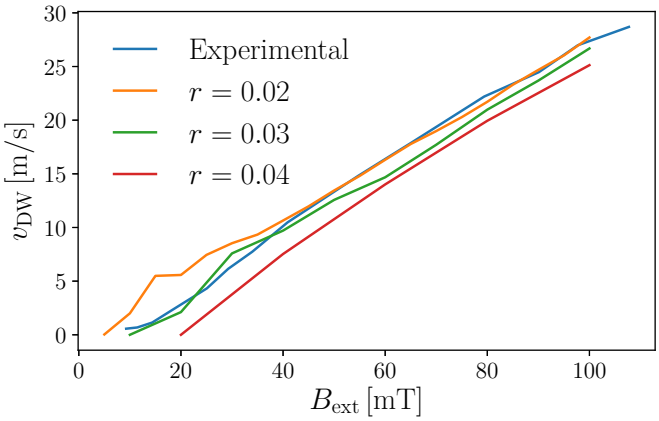

Figure 5.1. Domain wall velocity as a function of applied field $v_{\mathrm{DW}}(B_{\mathrm{ext}})$ w.r.t. different thickness variation values r compared to the experimental data by Metaxas *et al.* [50]. It can be seen that $r = 0.03$ gives best match in the field range of 10–40 mT, which is the range where we are going to drive the DW.

remains within one simulation cell from the DW position to minimize the effects of the demagnetizing field. In the original implementation there is a two cell tolerance to both directions around the window center. Simulation cell dimensions are $\Delta_x = \Delta_y = 2$ nm and $\Delta_z = 0.5$ nm. We used periodic boundary conditions in the y-direction to get rid of edge effects. Initially we set a $+y$ Bloch wall in the center of the sample with $\pm z$ domains, and relax the system into its equilibrium configuration under zero field. The field is applied in the$+z$-direction, when driving the system.

We introduce disorder in a form of thickness variation of the film and use Voronoi tessellation to define the grain geometries with the average grain size of 20 nm. Thickness of a grain is determined by $t_{\mathrm{G}} = h + \mathcal{N}(0,1)rh$, where t_{G} is the grain thickness, r the magnitude of the variation, and $h = 0.5$ nm is the average thickness of the sample. t_{G} is not applied to geometric thickness of grains but to the micromagnetic parameters of grains to simulate the thickness variation. To this end, saturation magnetization of the grain is set to $M_{\mathrm{S}}^{\mathrm{G}} = M_{\mathrm{S}} t_{\mathrm{G}}/h$ and the uniaxial anisotropy to $K_{\mathrm{u}}^{\mathrm{G}} = K_{\mathrm{u}} h/t_{\mathrm{G}}$ [51].

By scanning different values of r we achieve similar $v_{\mathrm{DW}}(B_{\mathrm{ext}})$ behavior to that reported by Metaxas *et al.* [50] for a 0.5 nm thick sample in the field range 0 – 30 mT. The results are shown in Fig. 5.1. It should be noted that the original experiments were conducted in finite temperature $T \approx 300$ K and our simulations are carried out in $T = 0$ K, which means that our results in Fig. 5.1 are not one-to-one comparable with the experiments.

The moving simulation window will remove any effects of the demagnetizing field slowing down the DW, but we "re-introduce" the slowing effect in a controllable fashion by driving the DW with a quasistatic constant velocity. The

constant velocity allows us to characterize the stationary avalanche time series using probability distributions. We use a threshold velocity of $v_{\mathrm{DW}}^{\mathrm{th}} = 0.1$ m/s to control the applied field. If the velocity is above the threshold, the field is decreased at a rate of $\dot{B}_{\mathrm{ext}} = -k|v_{\mathrm{DW}}|$, where $k = 0.18\,\mathrm{mT/nm}$. If v_{DW} is below the limit, the field is ramped up at a rate of $\dot{B}_{\mathrm{ext}} = 0.037\,\mathrm{mT/ns}$. The simulation time step is on the average $\langle \Delta_t \rangle \approx 2.7 \times 10^{-13}$ s. The k-parameter was adjusted so that the lateral size of the biggest avalanche was smaller than the length of the DW in order to avoid finite size effects, and the increase rate was balanced so that we get distinguishable avalanches from the velocity signal and the waiting time between avalanches is not excessively long. We used Dormand-Prince solver (RK45) with an adaptive time step.

To solve the domain wall velocity $v_{\mathrm{DW}}(t)$, we determine the DW position as $\mathbf{X}(\mathbf{y}) = \min_{\mathbf{y}} |\mathbf{m}_z(\mathbf{x})|$. Magnetization $m_{z,i}(x)$ is interpolated across the two points $x_{-1,i}$ and $x_{+1,i}$, where $\mathrm{sign}[m_{z,i}(x_{-1,i})] \neq \mathrm{sign}[m_{z,i}(x_{+1,i})]$, and we get the interpolated location of the domain wall $x_{0,i}$, that is $x_{-1,i} \leq x_{0,i} \leq x_{+1,i}$.

To quantify the activity of the internal DW dynamics and the activity related to the DW motion, we determine the in-plane activity A_{xy} and the out-of-plane activity A_z. We use the definitions

$$A_{xy}(t) = \sum_{i \in B} \dot{\phi}_i \cdot |\mathbf{m}_{xy,i}| \tag{5.1}$$

$$A_z(t) = \sum_{i \in B} \dot{\theta}_i, \tag{5.2}$$

where ϕ_i and θ_i are the spherical coordinate angles of the magnetization vector $\mathbf{m}_i$ in ith cell, and the dot denotes time derivative. B is a band extending 20 discretization cells around the DW on both sides and is moving along the DW. The second term in A_{xy} is used to suppress the effect of in-plane components in the domains, which would otherwise dominate the in-plane activity. The time derivatives are calculated using finite differences on the time scale of 1000 time steps, which is around 0.27 ns. We consider 200 realizations of the disorder for the analysis presented in the next section.

5.3 Results

5.3.1 Domain wall dynamics

First we analyze v_{DW} under static external field B_{ext} to find the depinning field of the system and to determine the type of dynamics the DW experiences in this field region. The results are presented in Fig. 5.2. The simulations were done with perfect and disordered ($r = 0.03$) Co film presented in red triangles and black circles, respectively. We can see that the depinning field of 15 mT is higher than the Walker field, which is around 2.5 mT. This confirms that the DW is experiencing precessional motion in the disordered system when the DW

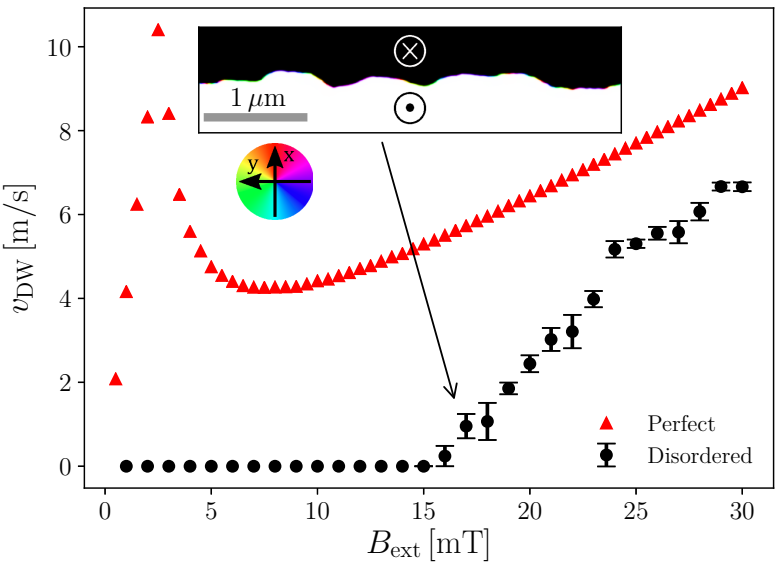

Figure 5.2. Average velocity of the DW subject to a static field $v_{\mathrm{DW}}(B_{\mathrm{ext}})$. The velocity of perfect film shows that DW motion in the disordered film ($r = 0.03$) is always precessional, because the depinning field is above the Walker field. The inset shows a snapshot of the DW magnetization and $\pm z$ domains surrounding the DW. It shows that the DW has nucleated some VBLs. The colorwheel depicts the mapping between the magnetization direction and the colors. Black and white colors correspond to $-z$ and $+z$ magnetizations, respectively.

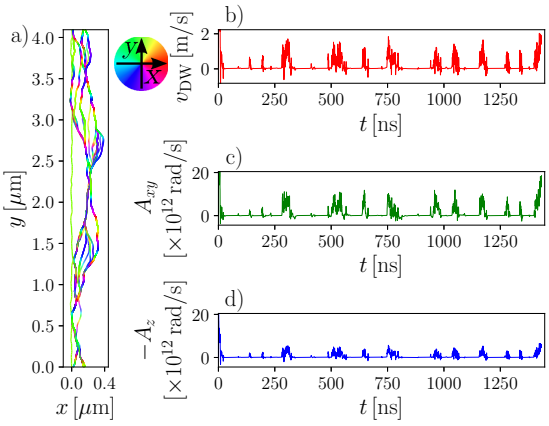

Figure 5.3. The domain wall spatial and magnetization configurations between avalanches are shown in a). The avalanches are determined from the velocity signal v_{DW} in b). The DW advances in abrupt jumps typical to Barkhausen effect. The activity signals $A_{xy}(t)$ and $-A_z(t)$ in c) and d), respectively, show that the magnetization evolves in bursts similar to what is seen in $v_{\mathrm{DW}}(t)$.

is depinned. This matter was unclear for Metaxas *et al.* [50] at the time of publishing the article. The nucleation of BLs can be confirmed from the inset of Fig. 5.2, which shows the magnetization after 37 ns after applying the field $B_{\mathrm{ext}} = 17\,\mathrm{mT}$.

After confirming the type of internal DW dynamics we can now move on to the DW dynamics when driven by the quasistatic constant velocity drive. A large number of BLs is nucleated in the DW shortly after the driving field is applied to the film, which can be seen in Fig. 5.3a). It shows the DW magnetizations between avalanches. The $+z$ domain is on the $-x$ side of the DW and the $-z$ domain is on the right side of the DW. The relaxed initial magnetization is the leftmost green DW front. It is evident that the in-plane magnetization of the DW is active during the DW jumps. The DW velocity v_{DW}, in-plane and out-of-plane activities A_{xy} and $-A_z$ in Fig. 5.3b), c) and d), respectively, all exhibit a bursty character typical of the Barkhausen effect. Notice the minus sign in the A_z signal, which is added to get better comparability between the activity signals. The angle θ tends rotate clockwise when the DW is advancing to $+x$-direction and driven with a $+z$ field. From Figs. 5.3c) and d) we can see that during the avalanches the magnitude of the in-plane activity is higher than the out-of-plane activity. It is actually higher by $\langle A_{xy}/A_z \rangle \approx 1.7$, which is averaged over 60 signals similar to the ones presented in Fig. 5.3. Between the avalanches the magnitude of A_{xy} is lower that of $-A_z$.

5.3.2 Avalanche initiation angle

Micromagnetics provides us the possibility to get insights about the magnetization conditions related to initiation of an avalanche, which is not possible

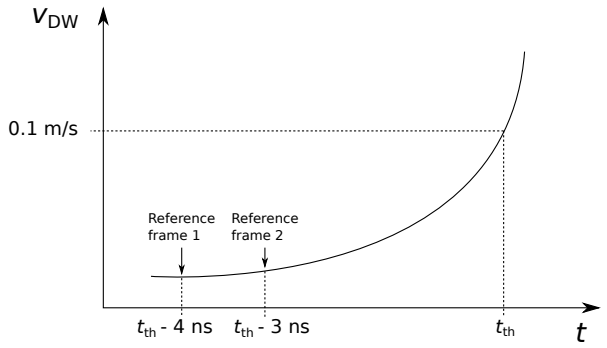

Figure 5.4. A schematic representation of the reference frames. The avalanche is considered triggered at time t_{th}. The segment of the DW, which has moved the most between *Reference frame 1* and *Reference frame 2*, is considered as the point where the avalanche was triggered.

with other computational methods. This type of experiment might be incredibly hard to conduct due to the limitations of both spatial and temporal resolution in magnetic imaging techniques. It is known that during the DW propagation the region of DW with a VBL is retarding the motion relative to the rest of the DW [23]. Thus, a heuristic guess would be that the avalanches tend to be initiated from segments of the DW without BLs.

The initiation point is determined as a segment of the DW, where the DW has moved the most looking back 4 ns before the time point where v_{DW} first goes above the threshold velocity $v_{\mathrm{DW}}^{\mathrm{th}} = 0.1$ m/s, and comparing it to 3 ns before the crossover. The selection of the reference frames are schematically presented in Fig. 5.4 and mathematical formulation of the initiation point y-coordinate of the DW segment is

$$y_{\mathrm{DW}}^{\mathrm{init}} = y_{\mathrm{DW}}\left\{\max\left[\mathbf{x}_{\mathrm{DW}}(t_{\mathrm{th}} - 3\,\mathrm{ns}) - \mathbf{x}_{\mathrm{DW}}(t_{\mathrm{th}} - 4\,\mathrm{ns})\right]\right\}, \tag{5.3}$$

where DW subscript stands for restricting the inspection only to discretization cells within the DW, and $\mathbf{x}_{\mathrm{DW}}$ is the x-coordinate of the DW position. Thus, the magnetization of the initiation point is $\mathbf{m}\left(x_{\mathrm{DW}}^{\mathrm{init}}, y_{\mathrm{DW}}^{\mathrm{init}}\right)$, where $x_{\mathrm{DW}}^{\mathrm{init}}$ is determined from Eq. (5.3) by replacing y_{DW} with x_{DW}.

Choosing 4 ns before the crossing is reasonable, because the DW is actually in motion already when $v_{\mathrm{DW}} < 0.1\,\mathrm{m/s}$ and the BLs are already moving at that point. Looking back a bit further ensures that the DW is at rest in the reference frame. We show the probability distribution of the in-plane angle of the DW segment where an avalanche is initiated in Fig. 5.5. The in-plane initiation angle probability distribution $P(\phi_{\mathrm{initial}})$ seems to follow quite well the domain wall magnetization distribution $P(\phi_{\mathrm{DW}})$ over all the corresponding DW magnetization configurations. This suggests that the nucleation is not correlated with the local magnetic structure of the DW.

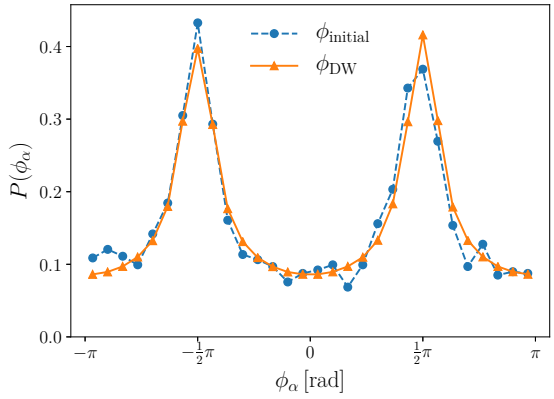

Figure 5.5. The probability distribution of in-plane magnetization directions of the DW ϕ_{DW} and probability distribution of the avalanche initiation point magnetization directions ϕ_{initial}. The initiation point is defined as the point, that has moved the most after 1 ns compared to a reference frame. 4 ns before an avalanche is nucleated ($v_{\text{DW}}(t) > v_{\text{DW}}^{th} = 0.1\,\text{m/s}$) is used as a reference frame.

5.3.3 Avalanche statistics

Let us now consider the statistics of bursty signals v_{DW}, A_{xy} and $-A_z$. Examples of these signals are presented in Figs. 5.3b), c) and d). It can be seen that all of the signals get negative values, and in case of v_{DW} and $-A_z$, this means that the DW center of mass is momentarily moving backwards. This on the other hand suggests that the DW does not seem to respect the Middleton theorem applicable for elastic interfaces in random medium [52].

To analyze the Barkhausen avalanches in our system we need to consider the avalanche size for all of the three signals. Let's denote the signal as $V(t)$ for simplicity as the analysis is the same for all of them. Thus the avalanche size is

$$S_V = \int_0^T \left[V(t) - V^{\text{th}} \right] dt, \tag{5.4}$$

where V^{th} is a signal threshold used to determine whether an avalanche is active. T is the duration of the avalanche and in this time period $V(t) > V^{\text{th}}$ holds. Avalanche size distributions $P(S_{A_z})$ and $P(S_{A_{xy}})$ are presented in Figs. 5.6a) and b) for different threshold values A_z^{th} and A_{xy}^{th}. The distributions can be well-described with a power law distribution with a cut-off $P(S_V) = S_V^{-\tau_S} f(S_V/S_V^*)$, where τ_S is a scaling exponent, $f(x)$ is a scaling function describing the shape of the cut-off, and S_V^* is the cut-off avalanche size. Avalanche duration distributions follow a similar scaling form.

We observe that the scaling exponents of the avalanche size and duration $\tau_S \approx 1.1$ and $\tau_T \approx 1.2$, respectively, are close to the values expected for the quenched Edwards Wilkinson (qEW) equation describing a short-range elastic string in a random medium [53]. We can also see that the cut-off avalanche

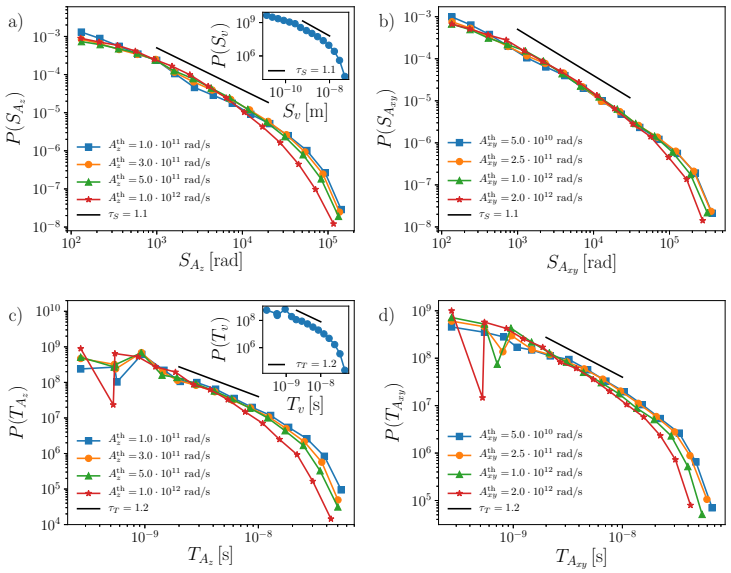

Figure 5.6. Distributions of avalanche sizes obtained from magnetization activity A_z signal in a) and b) A_{xy} signal. The applied avalanche signal A_z^{th} and A_{xy}^{th} thresholds are presented in the legends. The insets in a) and c) show corresponding avalanches size and duration distributions obtained for v_{DW} signal with 0.1 m/s threshold.

size and duration depend on the chosen threshold, but they seem to saturate to a value set by the artificial demagnetizing factor k. Insets in Figs. 5.6a) and c) show the distributions $P(S_v)$ and $P(T_v)$, extracted from the v_{DW} signal with $v_{\mathrm{DW}}^{\mathrm{th}} = 0.1$ m/s. The scaling exponent values seem to be very close to the values obtained from the two activity signals.

Fig. 5.7 shows the scaling of the average avalanche size as a function of the avalanche duration, $\langle S_{A_z}(T)\rangle$ in a) and $\langle S_{A_{xy}}(T)\rangle$ in b). We expect that the scaling behaves as $\langle S_{A_z}\rangle \sim T^{\gamma}$, where γ is the effective exponent describing the scaling (same applies to $\langle S_{A_{xy}}(T)\rangle$). We find that γ depends on the threshold values as was discovered recently for crack line propagation [54] and random field Ising model [55]. For the smallest thresholds for both $\langle S_{A_z}(T)\rangle$ and $\langle S_{A_{xy}}(T)\rangle$ we find $\gamma \approx 1.7$, which is relatively close to 1.6 expected for qEW equation in the limit of zero threshold [56]. The inset in Fig. 5.7a) shows $\langle S_v(T)\rangle$ for the data extracted from v_{DW}, with a slightly lower γ probably due to the relatively high value of the threshold.

5.4 Discussion

We have shown with a novel method in this context the significance of internal dynamics of the DW during its bursty propagation when driven in a disordered

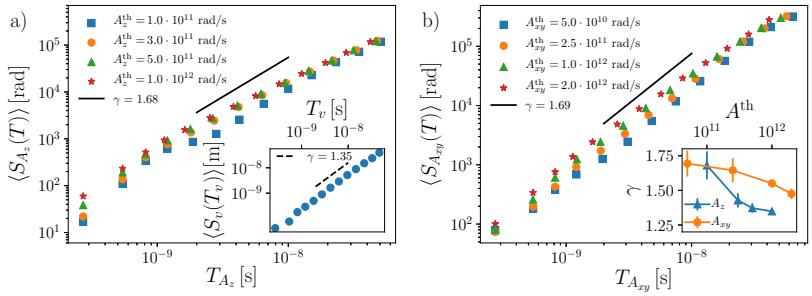

Figure 5.7. Scaling of the average avalanche size w.r.t. the avalanche duration for out-of-plane activity $\langle S_{A_z}(T) \rangle$ in a) and in-plane activity in $\langle S_{A_{xy}}(T) \rangle$ b) for different avalanche thresholds. The inset in a) shows the corresponding scaling obtained from the v_{DW} signal with $v_{\mathrm{DW}}^{\mathrm{th}} = 0.1$ m/s. The inset in b) shows the scaling exponents as a function of thresholds for the activity avalanches.

medium. We showed the magnetization rotation occurring during the avalanches is actually more significant in the in-plane components of the magnetization than in the movement of the DW. Surprisingly the power law properties of the avalanches in both the in-plane and out-of-plane activities show similar scaling exponents as the classical domain wall velocity signal, and they seem to be in good agreement with the much simpler qEW equation. The same ultrathin Pt/Co/Pt samples have been studied from creep point of view experimentally [15, 50, 57], and using the qEW equation [58], where a similar avalanche size exponent was reported. However, the critical exponents for avalanche size and duration distributions have not been measured experimentally for this material.

The VBLs produce dipolar fields decaying as $1/r^3$, which results in a short-ranged interactions for a one-dimensional elastic interface in a random medium. Such an interaction is not expected to change the universality class of the avalanche dynamics of an elastic line in random media from that of a line with purely local elasticity.

We also found that the local magnetization of the DW (VBLs in particular), does not affect the triggering probability. Although, it is known that the magnetization of VBL segments in general cause a local drag to a moving DW [24].

We suggest that this approach should be taken into 3D samples with 2D DWs and find out if the system still shows similar properties in the higher dimension. It would also be interesting to study the effect of Dzyaloshinskii-Moriya interaction [16] on the avalanche statistics and triggering mechanism.

6. Summary and outline

In this dissertation I have studied the effect of BLs on DW dynamics by utilizing the micromagnetics software MuMax3. The effects of BLs was studied in 2D disordered media as well as in perfect 3D samples. Before our work in Publication I BLs had been mostly neglected in the most recent work in the field of micromagnetics and DW dynamics.

In Publication I we studied the effect of the Bloch lines on domain wall velocity as well as the dynamics of the BLs. We showed a method to confine a DW for the purpose of studying BL dynamics. The BLs were then driven within the pinned DW and we found that the BLs can reach relatively high velocities without experiencing any breakdown due to the topological protection of the surrounding magnetic domains. We also showed that the BLs can be driven with an electrical current and can reach even higher velocities than field driven BLs. An experimental replication of our results especially in the case of the current driven BLs would be an interesting subject for future research.

In Publication II we studied the BL dynamics in 3D garnet samples. We verified theoretical results of sample thickness effects on the DW velocity in both thin and thick samples. We found that the local maximum velocity at the "intermediate" thickness was related to the space needed to accommodate a whole HBL with full π rotation as well as the critical points. The dynamics of DWs and BLs in disordered 3D samples was left for future research.

In Publication III we took a novel approach to DW avalanche dynamics with the micromagnetic implementation, which allowed us to study the internal magnetization of the DW during avalanches. We showed that the activity of the internal magnetization of the DW exhibited bursty evolution in time similar to the DW velocity signal. The avalanche statistics were in good agreement with a much simpler model that does not take the internal magnetization of the DW into account. We also showed that the magnetization of the avalanche triggering site is not correlated with the nucleation probability. The addition of Dzyaloshinskii-Moriya interaction would provide an interesting angle on the Barkhausen noise analysis done using micromagnetic simulations.

References

[1] B. D. Cullity and C. D. Graham. *Introduction to magnetic materials*. John Wiley & Sons, 2011.

[2] A. Hubert and R. Schäfer. *Magnetic domains: the analysis of magnetic microstructures*. Springer Science & Business Media, 1998.

[3] G. Tatara, H. Kohno, and J. Shibata. Microscopic approach to current-driven domain wall dynamics. *Physics Reports*, 468(6):213–301, 2008.

[4] Z. Li and S. Zhang. Domain-wall dynamics driven by adiabatic spin-transfer torques. *Physical Review B*, 70(2):024417, 2004.

[5] S. S. P. Parkin, M. Hayashi, and L. Thomas. Magnetic domain-wall racetrack memory. *Science*, 320(5873):190–194, 2008.

[6] S. S. P. Parkin and S-H. Yang. Memory on the racetrack. *Nature nanotechnology*, 10(3):195–198, 2015.

[7] S. S. P. Parkin, L. Thomas, M. Hayashi, and R. Moriya. Racetrack memory: the future of data storage. `http://www-03.ibm.com/ibm/history/ibm100/us/en/icons/racetrack/`, 2018. [Online; accessed 25-May-2018].

[8] S-H. Yang, K-S. Ryu, and S. S. P. Parkin. Domain-wall velocities of up to 750 m s- 1 driven by exchange-coupling torque in synthetic antiferromagnets. *Nature nanotechnology*, 2015.

[9] R. A. Duine, K-J. Lee, S. S. P. Parkin, and M. D. Stiles. Synthetic antiferromagnetic spintronics. *Nature Physics*, page 1, 2018.

[10] E. Martinez. The stochastic nature of the domain wall motion along high perpendicular anisotropy strips with surface roughness. *Journal of Physics: Condensed Matter*, 24(2):024206, 2012.

[11] T. Herranen and L. Laurson. Domain walls within domain walls in wide ferromagnetic strips. *Physical Review B*, 92(10):100405, 2015.

[12] M. Bode, E. Y. Vedmedenko, K. Von Bergmann, A. Kubetzka, P. Ferriani, S. Heinze, and R. Wiesendanger. Atomic spin structure of antiferromagnetic domain walls. *Nature materials*, 5(6):477, 2006.

[13] J. F. Dillon Jr and H. E. Earl Jr. Domain wall motion and ferrimagnetic resonance in a manganese ferrite. *Journal of Applied Physics*, 30(2):202–213, 1959.

[14] G. Gavoille and J. Hubsch. Fractal model for disordered magnets. *Physical Review B*, 37(1):321, 1988.

[15] S. Lemerle, J. Ferré, C. Chappert, V. Mathet, T. Giamarchi, and P. Le Doussal. Domain wall creep in an ising ultrathin magnetic film. *Physical Review Letters*, 80:849–852, Jan 1998.

[16] Y. Yoshimura, K-J. Kim, T. Taniguchi, T. Tono, K. Ueda, R. Hiramatsu, T. Moriyama, K. Yamada, Y. Nakatani, and T. Ono. Soliton-like magnetic domain wall motion induced by the interfacial dzyaloshinskii-moriya interaction. *Nature Physics*, 12(2):157–161, 2016.

[17] G. Durin and S. Zapperi. The barkhausen effect. *The Science of Hysteresis: Physical modeling, micromagnetics, and magnetization dynamics*, 2:181, 2006.

[18] D. A. Allwood, G. Xiong, C. C. Faulkner, D. Atkinson, D. Petit, and R. P. Cowburn. Magnetic domain-wall logic. *Science*, 309(5741):1688–1692, 2005.

[19] J. H. Franken, H. J. M. Swagten, and B. Koopmans. Shift registers based on magnetic domain wall ratchets with perpendicular anisotropy. *Nature nanotechnology*, 7(8):499, 2012.

[20] A. Mougin, M. Cormier, J. P. Adam, P. J. Metaxas, and J. Ferré. Domain wall mobility, stability and walker breakdown in magnetic nanowires. *EPL (Europhysics Letters)*, 78(5):57007, 2007.

[21] N. L. Schryer and L. R. Walker. The motion of 180 domain walls in uniform dc magnetic fields. *Journal of Applied Physics*, 45(12):5406–5421, 1974.

[22] L. Thomas, M. Hayashi, X. Jiang, R. Moriya, C. Rettner, and S. S. P. Parkin. Oscillatory dependence of current-driven magnetic domain wall motion on current pulse length. *Nature*, 443(7108):197–200, 2006.

[23] J. C. Slonczewski. Theory of domain-wall motion in magnetic films and platelets. *Journal of Applied Physics*, 44(4):1759–1770, 1973.

[24] A. P. Malozemoff and J. C. Slonczewski. *Magnetic Domain Walls in Bubble Materials: Advances in Materials and Device Research*, volume 1. Academic Press, New York, 1979.

[25] S-K. Kim, J-Y. Lee, Y-S. Choi, K. Y. Guslienko, and K-S. Lee. Underlying mechanism of domain-wall motions in soft magnetic thin-film nanostripes beyond the velocity-breakdown regime. *Applied Physics Letters*, 93(5):052503, 2008.

[26] H-B. Braun. Topological effects in nanomagnetism: from superparamagnetism to chiral quantum solitons. *Advances in Physics*, 61(1):1–116, 2012.

[27] T. Herranen and L. Laurson. Bloch-line dynamics within moving domain walls in 3d ferromagnets. *Physical Review B*, 96(14):144422, 2017.

[28] B. MacNeal and F. Humphrey. Horizontal bloch line motion in magnetic bubble materials. *IEEE Transactions on Magnetics*, 15(5):1272–1284, 1979.

[29] H. Barkhausen. Zwei mit hilfe der neuen verstärker entdeckte erscheinungen. *Phys. Z*, 20:401, 1919.

[30] W. C. Elmore. The magnetic structure of cobalt. *Physical Review*, 53:757–764, May 1938.

[31] S. Zapperi, P. Cizeau, G. Durin, and H. E. Stanley. Dynamics of a ferromagnetic domain wall: Avalanches, depinning transition, and the barkhausen effect. *Physical Review B*, 58(10):6353, 1998.

[32] J. Anglada-Rivera, L. R. Padovese, and J. Capo-Sanchez. Magnetic barkhausen noise and hysteresis loop in commercial carbon steel: influence of applied tensile stress and grain size. *Journal of magnetism and magnetic materials*, 231(2):299–306, 2001.

[33] V. Moorthy, B. A. Shaw, and J. T. Evans. Evaluation of tempering induced changes in the hardness profile of case-carburised en36 steel using magnetic barkhausen noise analysis. *Ndt & E International*, 36(1):43–49, 2003.

[34] A. Vansteenkiste, J. Leliaert, M. Dvornik, M. Helsen, F. Garcia-Sanchez, and B. Van Waeyenberge. The design and verification of mumax3. *Aip Advances*, 4(10):107133, 2014.

[35] A. Vansteenkiste. GitHub - MuMax3. `https://github.com/mumax/3/releases`, 2018. [Online; accessed 24-May-2018].

[36] S. Zhang and Z. Li. Roles of nonequilibrium conduction electrons on the magnetization dynamics of ferromagnets. *Physical Review Letters*, 93(12):127204, 2004.

[37] J. C. Slonczewski. Current-driven excitation of magnetic multilayers. *Journal of Magnetism and Magnetic Materials*, 159(1-2):L1–L7, 1996.

[38] Y. Kubota, L. Folks, and E. E. Marinero. Intergrain magnetic coupling and microstructure in coptcr, coptcrta, and coptcrb alloys. *Journal of applied physics*, 84(11):6202–6207, 1998.

[39] O. Boulle, S. Rohart, L. D. Buda-Prejbeanu, E. Jué, I. M. Miron, S. Pizzini, J. Vogel, G. Gaudin, and A. Thiaville. Domain wall tilting in the presence of the dzyaloshinskii-moriya interaction in out-of-plane magnetized magnetic nanotracks. *Physical review letters*, 111(21):217203, 2013.

[40] M. Voto, L. Lopez-Diaz, L. Torres, and S. Moretti. Disorder-induced domain wall velocity shift at high fields in perpendicularly magnetized thin films. *Physical Review B*, 94(17):174438, 2016.

[41] A. S. Logginov, A. V. Nikolaev, and V. V. Dobrovitski. Direct optical observation of vertical bloch lines propagation by in-plane field pulses. *IEEE transactions on magnetics*, 29(6):2590–2592, 1993.

[42] J. Leliaert, M. Dvornik, J. Mulkers, J. De Clercq, M. V. Milošević, and B. Van Waeyenberge. Fast micromagnetic simulations on gpu — recent advances made with mumax3. *Journal of Physics D: Applied Physics*, 51(12):123002, 2018.

[43] A. Thiaville, J. Miltat, and J. B. Youssef. Dynamics of vertical bloch lines in bubble garnets: Experiments and theory. *The European Physical Journal B-Condensed Matter and Complex Systems*, 23(1):37–47, 2001.

[44] E. Schlömann. Domain walls in bubble films. iii. wall structure of stripe domains. *Journal of Applied Physics*, 45(1):369–373, 1974.

[45] M. Redjdal and F. B. Humphrey. Simulation of three-dimensional nonperiodic structures of π-vertical bloch line and 2π-vertical bloch line in magnetic garnet. *Journal of applied physics*, 79(8):6464–6466, 1996.

[46] A. Bagneres and F. B. Humphrey. Dynamics of magnetic domain walls with loosely spaced vertical bloch lines. *IEEE transactions on magnetics*, 28(5):2344–2346, 1992.

[47] F-U. Stein, L. Bocklage, M. Weigand, and G. Meier. Time-resolved imaging of nonlinear magnetic domain-wall dynamics in ferromagnetic nanowires. *Scientific reports*, 3:1737, 2013.

[48] L. Xiong, B. Zheng, M.H. Jin, L. Wang, and N. J. Zhou. Dynamic depinning phase transition in magnetic thin film with anisotropy. *New Journal of Physics*, 20(2):023027, 2018.

[49] L. D. Geng and Y. M. Jin. Domain wall creep in magnetic thin films near the depinning transition. *EPL (Europhysics Letters)*, 116(3):36002, 2016.

[50] P. J. Metaxas, J. P. Jamet, A. Mougin, M. Cormier, J. Ferré, V. Baltz, B. Rodmacq, B. Dieny, and R. L. Stamps. Creep and flow regimes of magnetic domain-wall motion in ultrathin pt/co/pt films with perpendicular anisotropy. *Physical review letters*, 99(21):217208, 2007.

[51] S. Moretti, M. Voto, and E. Martinez. Dynamical depinning of chiral domain walls. *Physical Review B*, 96(5):054433, 2017.

[52] A. A. Middleton. Asymptotic uniqueness of the sliding state for charge-density waves. *Physical review letters*, 68(5):670, 1992.

[53] A. Rosso, P. Le Doussal, and K. J. Wiese. Avalanche-size distribution at the depinning transition: A numerical test of the theory. *Physical Review B*, 80(14):144204, 2009.

[54] S. Janićević, L. Laurson, K. J. Måløy, S. Santucci, and M. J. Alava. Interevent correlations from avalanches hiding below the detection threshold. *Physical review letters*, 117(23):230601, 2016.

[55] S. Janićević, D. Jovković, L. Laurson, and D. Spasojević. Threshold-induced correlations in the random field ising model. *Scientific reports*, 8(1):2571, 2018.

[56] L. Laurson, X. Illa, S. Santucci, K. T. Tallakstad, K. J. Måløy, and M. J. Alava. Evolution of the average avalanche shape with the universality class. *Nature communications*, 4:2927, 2013.

[57] J. Gorchon, S. Bustingorry, J. Ferré, V. Jeudy, A. B. Kolton, and T. Giamarchi. Pinning-dependent field-driven domain wall dynamics and thermal scaling in an ultrathin pt/co/pt magnetic film. *Physical review letters*, 113(2):027205, 2014.

[58] E. E. Ferrero, L. Foini, T. Giamarchi, A. B. Kolton, and A. Rosso. Spatiotemporal patterns in ultraslow domain wall creep dynamics. *Physical review letters*, 118(14):147208, 2017.

Aalto-DD 153/2018

ISBN 978-952-60-8133-5 (printed)
ISBN 978-952-60-8134-2 (pdf)
ISSN 1799-4934 (printed)
ISSN 1799-4942 (pdf)

Aalto University
School of Science
Department of Applied Physics
www.aalto.fi

BUSINESS +
ECONOMY

ART +
DESIGN +
ARCHITECTURE

SCIENCE +
TECHNOLOGY

CROSSOVER

DOCTORAL
DISSERTATIONS